RESEARCH ARTICLE

Architecture, structural and tectonic significance of the Seagap fault (offshore Tanzania) in the framework of the East African Rift

David Iacopini[1] | **Stefano Tavani**[1] | **Sara Pentagallo**[1] | **Vittorio Maselli**[2] | **Marina Dottore Stagna**[2] | **Cynthia Ebinger**[3] | **David Reynolds**[2] | **Arjan van Vliet**[4]

[1]Dipartimento di Scienze della Terra dell' Ambiente e delle Risorse (DISTAR), Università di Napoli Federico II, Naples, Italy

[2]Department of Earth and Environmental Sciences, Dalhousie University, Halifax, Nova Scotia, Canada

[3]Department of Earth and Environmental Sciences, Tulane University, New Orleans, Louisiana, USA

[4]Royal Dutch Shell, The Hague, The Netherlands

Correspondence
David Iacopini, DiSTAR, Università di Napoli Federico II, Naples, Italy.
Email: david.iacopini@unina.it

Funding information
University of Naples; Natural Sciences and Engineering Research Council of Canada, Grant/Award Number: RGPIN-2020-04461; National Science Foundation, Grant/Award Number: EAR-2039963

Abstract

The Southeastern portion of the East African Rift System reactivates Mesozoic transform faults marking the separation of Madagascar from Africa in the Western Indian Ocean. Earlier studies noted the reactivation of the Davie Fracture Zone in oceanic lithosphere as a seismically active extensional fault, and new 3D seismic reflection data and exploration wells provide unprecedented detail on the kinematics of the sub-parallel Seagap fault zone in continental/transitional crust landward of the ocean-continent transition. We reconstruct the evolution of the seismically active Seagap fault zone, a 400-km-long crustal structure affecting the Tanzania margin, from the late Eocene to the present day. The Seagap fault zone is represented by large-scale localized structures affecting the seafloor and displaying growth geometries across most of the Miocene sediments. The continuous tectonic activity evident by our seismic mapping, as well as 2D deep seismic data from literature, suggests that from the Middle-Late Jurassic until 125 Ma, the Seagap fault acted as a regional structure parallel to, and coeval with, the dextral Davie Fracture Zone. The Seagap fault then remained active after the cessation of both seafloor spreading in the Somali basin and strike-slip activity on the Davie Fracture Zone, till nowaday. Its architecture is structurally expressed through the sequence of releasing and restraining bends dating back at least to the early Neogene. Seismic sections and horizon maps indicate that those restraining bends are generated by strike-slip reactivation of Cretaceous structures till the Miocene. Finally based on the interpretation of edge-enhanced reflection seismic surfaces and seafloor data, we shows that, by the late Neogene, the Seagap fault zone switched to normal fault behaviour. We discuss the Seagap fault's geological and kinematic significance through time and its current role within the microplate system in the framework of the East African rift, as well as implications for the evolution and re-activation of structures along sheared margins. The newly integrated datasets reveal the polyphase deformation of this margin, highlighting

its complex evolution and the implications for depositional fairways and structural trap and seal changes through time, as well as potential hazards.

1 | INTRODUCTION

The Southeastern branch of the East African Rift System (EARS) involves extension of both stretched continental and oceanic lithosphere near the ocean-continent transition in the Western Indian Ocean (e.g. Phethean et al., 2016; Roche & Ringenbach, 2022; Sauter et al., 2018) (Figure 1). Although frequent Mw >6 earthquakes occur along the Southeastern rift and massive tsunamigenic landslides have been mapped in the near offshore, the East African continental margin represents a geologically poorly understood area (Figure 1). The N-S striking structures in the nearshore and offshore originated from the superposition of two rifting episodes related to the following: (1) During the Mesozoic, NNW–SSE and then N-S divergence occurred between Madagascar and East Africa, which led to the opening of the West Somali basin (WSB), floored by Mesozoic oceanic crust (e.g. Müller & Jokat, 2019; Phethean et al., 2016; Tuck-Martin et al., 2019); (2) Recent ca. E-W divergence between the Somalian Plate and the Rovuma Microplate in the framework of the EARS (Ebinger & Sleep, 1998; Franke et al., 2015; Saria et al., 2014; Stamps et al., 2014, 2020, 2021). The W-E divergence is also responsible for the transcurrent active plate boundary along the Comoros archipelago interpreted by Famin et al. (2020) as a right lateral transform. Overall, the area of investigation is characterized by three major sets of regional-scale structures: (1) a system of recent extensional structures (Coffin & Rabinowitz, 1987, 1992; Mougenot et al., 1986) whose orientation spans from NW-SE to N-S, including horst structures like the islands of Pemba and Zanzibar (Dottore Stagna et al., 2022); (2) the Davie Fracture Zone (DFZ), which represents a major structure, around 2000 km long (Scrutton, 1978), from the Kenya margin to the southwest Madagascar margin (Figure 1); (3) a poorly mapped structure known as Seagap fault zone (or Sea Gap, Reeves et al., 2016) and interpreted as a strike-slip fault (Reeves et al., 2016; Sinha et al., 2019), which parallels the DFZ. The Davie and Seagap faults together appear to retrace the Mesozoic Continent-Ocean Transition (Sauter et al., 2016, 2018) (Figure 1). While the extensional rift structures of the DFZ and

Highlights

- The Seagap fault zone represents a ca. 400-km long, regional structure affecting the offshore Tanzania margin.
- Seagap fault zone reactivates Cretaceous fracture system.
- From the Eocene through the early Neogene, the Seagap fault zone acted as a sinistral strike slip fault.
- In the late Neogene, the tectonic activity of the Seagap fault zone switched to normal offset, deforming the seafloor.

the Davie Ridge (DR) have been the primary research focus of the offshore Tanzania basin (see Roche & Ringenbach, 2022) first mentions and seismic images of the Seagap fault has been proposed only recently by conference reports (Pike et al., 2015; Sayers, 2016; Rego et al., 2019) and some review paper (MacGregor, 2015). Rego et al. (2019) state that this regional feature is a large sinistral transcurrent fault zone rooted in a crustal-scale re-activated Mesozoic rift structure in oceanic lithosphere. Sauter et al. (2018), based on seismic and gravity data, have proposed this structure as the western limit of the oceanic domain, at the boundary between the Rovuma Microplate and the Somalian Plate (Figure 1). Sansom (2018) using coherency time slices from 3D seismic reflection dataset, illustrated the effect of the Seagap fault in deflecting mid-Campanian and Turonian channels, therefore confirming its clear left-lateral offset between 94 and 72 Ma. Using a mapped seismic dataset from Exploration Block2 (Figure 2), Sadiki et al. (2021) confirmed the kinematic interpretation of the Seagap fault zone as a strike-slip fault that probably originated from the left-lateral reactivation of Albian rift structures. However, the above-cited authors present or regional 2D seismic sections imaging the Seagap structure or and propose sketch map views of the Seagap strike-slip system. Recent regional reconstruction by Sinha et al. (2019) and Roche and Ringenbach (2022) interpret the Seagap fault zone as part of the DFZ-wide
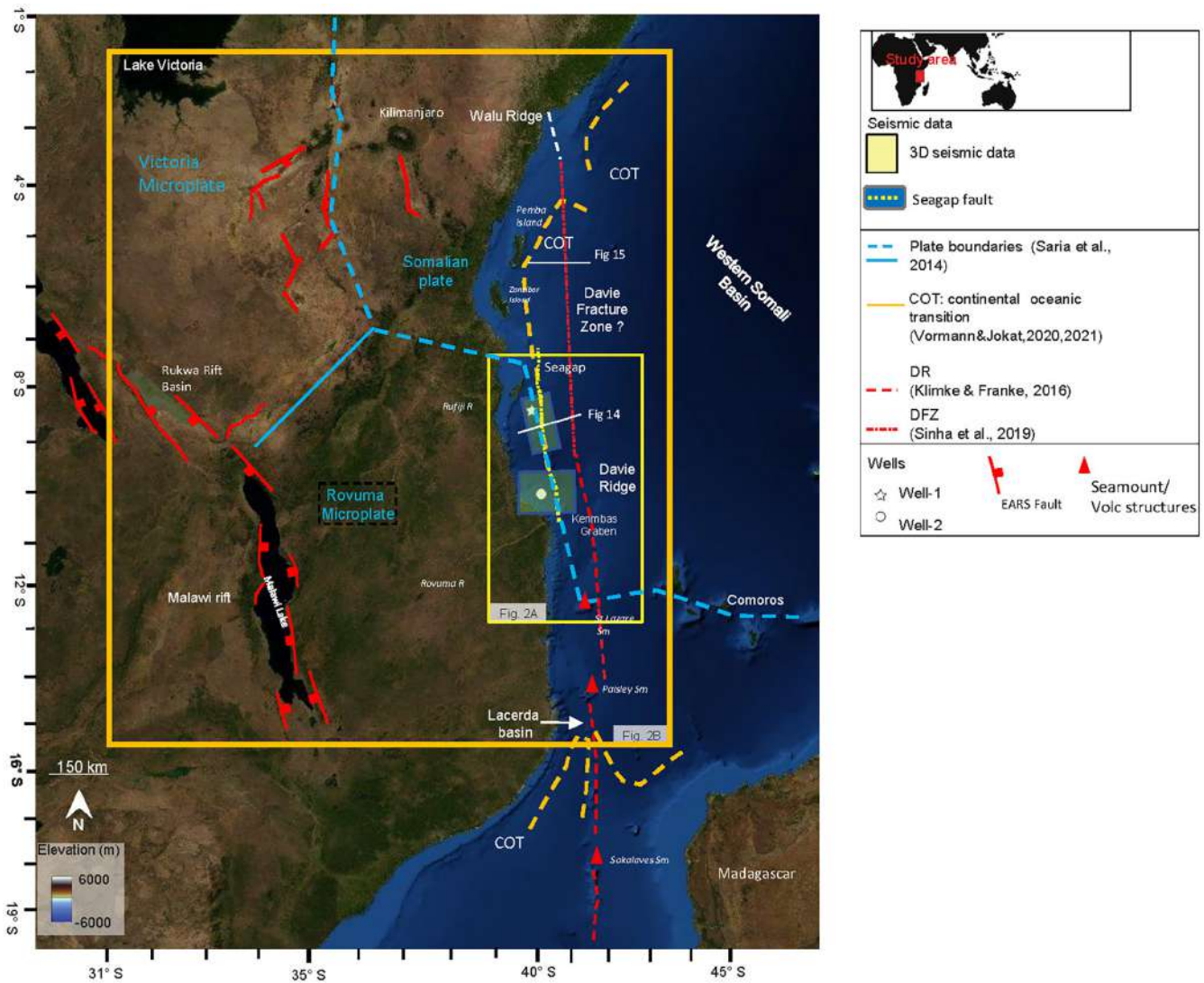
FIGURE 1 Outline and tectonic setting of the offshore Tanzania. The bathymetry is based on the GEBCO 2014 grid (version 20150318; Weatherall et al., 2015). Dashed and bold blue lines represent the inferred plate boundaries between Rovuma microplate, Somalian plate and Tanzania craton. Dashed orange boundaries represent the inferred ocean-continent transition boundary based Ségoufin et al. (2004), Sauter et al. (2018) and Vormann and Jokat (2021b) reconstructions. Dotted-dashed red line represent the Davie fracture zone, respectively, as by Klimke and Franke (2016) and Sinha et al. (2019). The two shaded yellow boxes, from north to south, represent the location of the Mafia and Kusini 3D datasets including the two wells 1 and 2.

deformation zone. In the Tanzania offshore region where geophysical constraints are still few, the deformation appears diffuse and delocalized. By using newly released 3D seismic datasets and exploration wells, we focus on the description of the architecture and main structural features characterizing the Seagap fault zone in two specific sectors offshore Tanzania (Figure 2), explore its timing and discuss its tectonic and kinematic significance from Late Eocene to Present within the offshore Somali basin. Our work serves to synthesize information on the Mesozoic-Recent kinematics of the Seagap fault zone, and it offers new insights into rejuvenation of transform faults along passive continental margins.

2 | REGIONAL SETTING

2.1 | The WSB crustal structure

Our study area is located in the WSB, between 8°S and 13°S offshore Tanzania (Figure 1). It is bounded on the west by the southern branch of the continental EARS marked by the Malawi and Rukawa rift zones, and by active and diffuse deformation within the DR on the east (e.g. Kusky et al., 2010; Stamps et al., 2020, 2021). The EARS represents a ca. 5000-km-long divergent boundary between the Nubian, Somalian and Arabian plates, as well as a number of smaller microplates including the Victoria, and Rovuma (Figure 1), some of which are
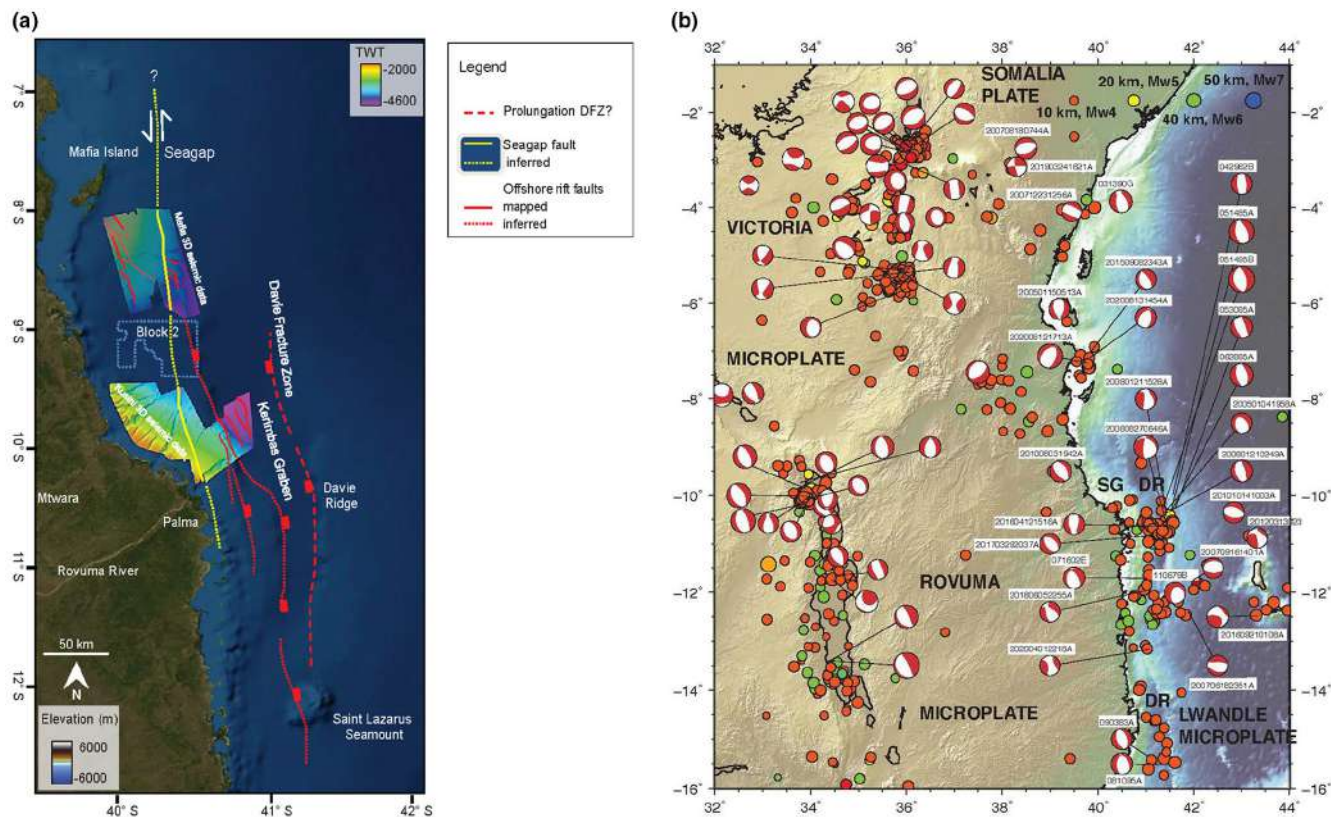
FIGURE 2 Regional tectonic offshore outline. (a) zoom of the working area, offshore Tanzania. The bathymetry is based on the GEBCO 2014 grid (version 20150318; Weatherall et al., 2015). The dotted-to-continuous yellow line represents the Seagap fault location; red line represents the outline of the arcuate NW to SE Neogene rift structures and dashed red line represents the inferred prosecution of the Davie Fracture. (b) Earthquake epicentres map from the USGS National Earthquake Information Center. The epicentre locations are coloured with respect to depth and scaled with respect to magnitude (scale on upper right). Earthquake sources for same time period from the Global Centroid Moment Tensor catalogue (Ekstrom et al., 2012).

cored by Archaean cratons (e.g. Daly et al., 2020; Stamps et al., 2020). The eastern branch of the East African rift is bounded on its western side by the Tanzania and Zimbabwe cratons. Opening of the WSB can be traced back to the Middle-Late Jurassic, when Madagascar separated from Africa (Davis et al., 2016; Geiger et al., 2004; Phethean et al., 2016; Rabinowitz et al., 1983; Sauter et al., 2018; Seton et al., 2012). Regional seismic and free air gravity and magnetic data (Ségoufin et al., 2004; Ségoufin & Patriat, 1980) indicate that the spreading in the WSB was initially directed NNW–SSE at around 170 Ma, but that it changed to N–S at around 150.5–155 Ma (Phethean et al., 2016). Müller and Jokat (2019) assign the change in relative plate motion to between chron M26r (157 Ma) and chron M18n (144 Ma). Seafloor spreading ceased at ca. 125 Ma (Phethean et al., 2016), although others propose an older age of cessation at 133.1–133.6 Ma (see Tuck-Martin et al., 2019). The changes in spreading direction between 132 and 120 Ma (Sauter et al., 2018) triggered intraplate deformation, folding of the oceanic crust and reactivating pre-Hauterivian structures by westward and eastward verging reverse

faulting and inversion. Deformation was localized in 15- to 30-km-wide zones (Sauter et al., 2018).

2.2 | The Ocean-Continental transition

The demarkation of the current ocean-continent boundaries still contains uncertainties as existing crustal-scale data are wholly 2-D (e.g. Roche & Ringenbach, 2022). Offshore Mozambique and Tanzania, there is still no agreement on the nature of the crustal structure (Figure 1). Sauter et al. (2016, 2018) using marine gravity data suggest the ocean-continent transition is delimited by the Seagap fault zone implying the DR cuts oceanic crust. Further south in the Mozambique Channel, Vormann and Jokat (2021b), Vormann et al. (2020) using velocity depth functions, suggest that the oceanic crust between 40.4°E and 40.9°E continues to 16.5°S (Figure 1). Eastwards to the DR, stretched continental crust links the DR to Madagascar. At 14.5°S the continental DR appears to separate oceanic crust of the Somali (east) (Figure 1) and Mozambique basins (west) while the transitional crustal

area at the central Mozambiquan margin is underlain by high velocity lower crust (HVLC) interpreted as magmatic underplate (Vormann et al., 2020). In the study area, the inferred Continent-Ocean Transition follows the N-S trend of the Davie and Seagap faults (Figure 1), suggesting that these plate-scale structures define, respectively, a transform plate boundary zone and the western margin of the oceanic basin (e.g. Roche & Ringenbach, 2022; Sauter et al., 2018).

2.3 | East African rifting and magmatism

Within and overprinting the above-cited pre-Aptian structures along offshore Tanzania, the rifted margin has evidence for early Neogene to Recent normal faulting, including numerous M > 4.5 earthquakes and faults that offset the seafloor (Coffin & Rabinowitz, 1987; Franke et al., 2015; Grimison & Chen, 1988; Mougenot et al., 1986). The discovery of abandoned deep-water channels of Neogene age along the crest of the DR and evidence of active faulting at the seafloor (Maselli et al., 2019) further demonstrates that this extensional activity can be traced to the early Miocene and is still active today (Bertil et al., 2021; Grimison & Chen, 1988). During the Miocene, normal faulting occurred along the Kenyan and Tanzanian coastal margins (e.g. Franke et al., 2015), creating topographic highs, such as Zanzibar, Pemba and Mafia Islands, and lows, such as the coastal basin and the Kerimba and Lacerda basins (Dottore Stagna et al., 2022; Kent et al., 1971; Mougenot et al., 1986). The Seagap fault zone is located along the western flank of the Davie Ridge and Kerimba Graben (Rego et al., 2019; Figure 2).

2.4 | DFZ: Structures and hypothesis

The seismically active DFZ, discovered by Heirtzler and Burroughs (1971), in the Western Somali basin and Mozambique basin is delineated by gravity and magnetic anomalies from 11°S to 21°S (Klimke & Franke, 2016; Phethean et al., 2016) and at the seafloor is expressed by a marked bathymetric ridge named the Davie Ridge (Franke et al., 2015). Dredge sampling (see ref in Mougenot et al., 1986) in the northern part of the DR suggests a composition mainly of sedimentary cover above flat basement. Dredge sampling in southern part recovered mainly continental rocks along the southern part of the DR (Bassias, 1992). Three undated volcanic structures are identified between 11°S and 19°S along the DR (the Paisley, St. Lazare and Sakalaves seamounts, Figure 1), and several studies relate these seamounts to Miocene-Recent volcanism (Courgeon et al., 2018; Deville et al., 2018; Mahanjane, 2014).

Alternatively, stratigraphic relations indicate that the Paisley and St Lazare seamounts formed in Cretaceous time (Franke et al., 2015; Mahanjane, 2014).

The DFZ is a complex, long-lived crustal structure (e.g. Bassias, 1992; Bassias & Leclaire, 1990; Klimke & Franke, 2016; Mahanjane, 2014; Roche & Ringenbach, 2022; Scrutton, 1978; Sinha et al., 2019; Vormann et al., 2020) with polyphase deformation that includes a large range of strike-slip structures. The DFZ was reactivated by localized extensional (e.g. Kerimbas and Lacerda Basin, see Maselli et al., 2020, Vormann & Jokat, 2021a) and contractional structures of Hauterivian-Aptian age (e.g. Intawong et al., 2019; Mahanjane, 2014, Roche & Ringenbach, 2022) (Figure 2). Grimison and Chen (1988) analysed a swarm of 5 < mb < 6.4 earthquakes with normal faulting mechanisms along N-S striking nodal planes, and they interpreted the Davie Ridge as the eastern edge of the EARS. Although gravity and magnetic anomalies and their derivatives have been used to link the south Somalian Wadu Ridge structure to the DFZ (Gaina et al., 2013; Reeves & de Wit, 2000), seismic reflection data do not show clear evidence of the DFZ north of 9° S (Klimke & Franke, 2016; Maselli et al., 2020; Sauter et al., 2018). Vormann et al. (2020) trace the DFZ south to 27°S latitude as a bathymetric ridge (Figures 1 and 2).

2.5 | Stratigraphy of the study area

Due to data limitations, the present study focuses data mapping on the post-Eocene stratigraphy, including the modern seafloor, and adopts the stratigraphy nomenclature and description proposed in the previous papers by Maselli et al. (2019, 2020). The area of investigation comprises a series of slope-deep water channel complexes which reflect both the sediment supply from the Ruaha/Rufiji and Rovuma rivers and the influence of the bottom currents which are northward directed (Sansom, 2018). By integrating seismic and gamma ray data from 2 wells, Maselli et al. (2020) identified 13 depositional cycles and defined three main units bounded by four horizons covering, from the base of the Eocene to the Quaternary, a 45-million-year time span including the reflectors M1, M2, M2a (Figure 3). From the Eocene, the offshore Tanzania passive margin has recorded a sediment influx initiated by plateau uplift (e.g. Ebinger & Sleep, 1998; Sembroni et al., 2016; van Wijk et al., 2021), by more regional rift flank uplift, and by the volcanic topographic changes which led to the progradation of the Rufiji and Rovuma river deltas and a deep-water drainage system (Figure 2). Offshore, from the middle to upper Miocene, the tectonic activity drove the uplift of the DFZ and the formation of the Kerimbas Graben, producing a clear re-routing of the deep-water drainage network in
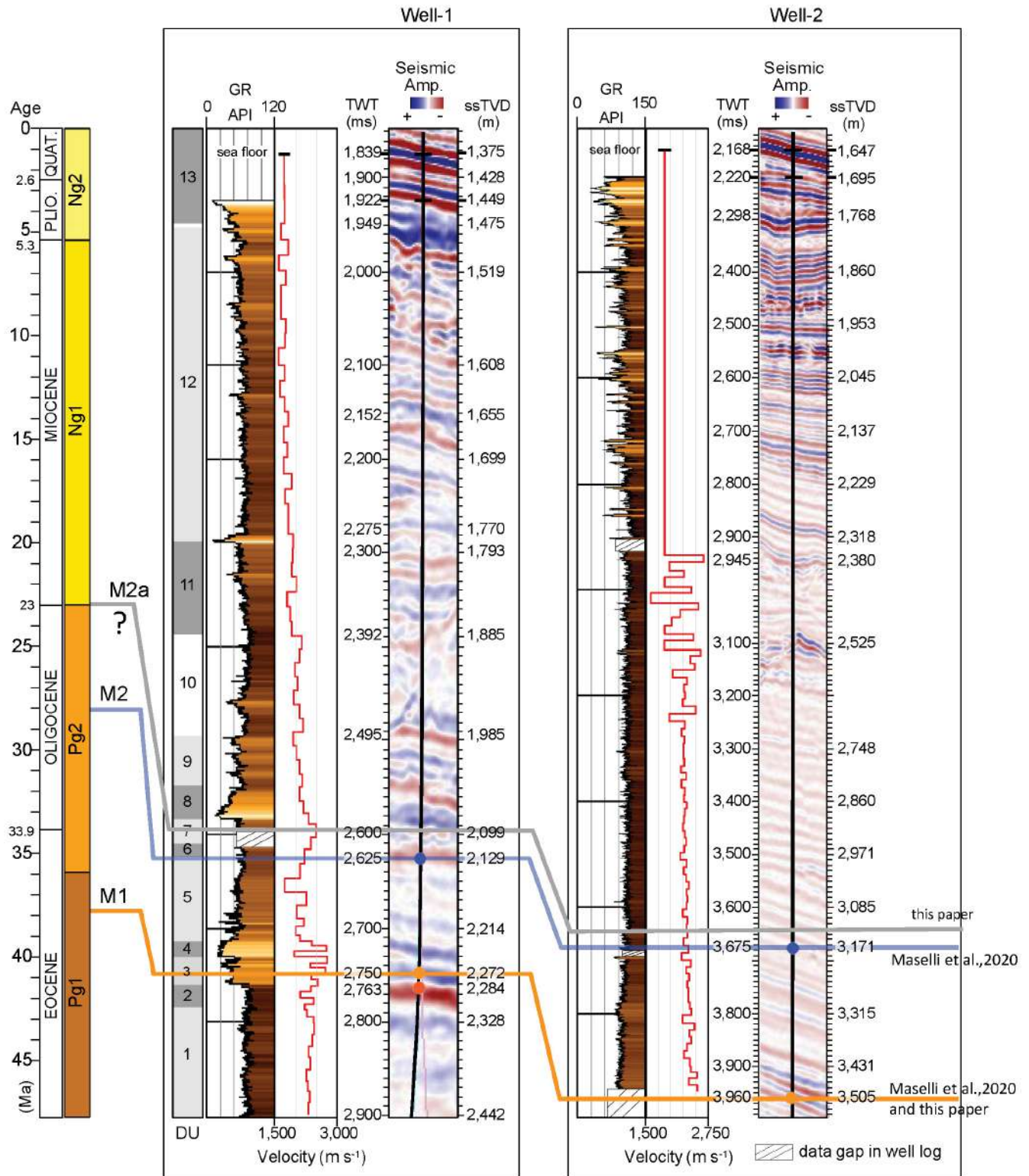
FIGURE 3 Well-to-seismic tie and biostratigraphy of Well-1 and Well-2. Well-to-seismic tie of Well-1 and Well-2 with dated stratigraphic horizons (M1-M2–M2a), seismic amplitude at the well sites, gamma-ray (GR), velocity model from check-shots, depth below sea level in two-way travel time (TWT, milliseconds) and true vertical depth (ssTVD, metres), and depositional units (DU) from Maselli et al. (2020). Stratigraphic sequences (Pg1 to Ng2) are from Sansom (2018).

the east part of the passive margin, which further modified the physiography of the margin (Maselli et al., 2019). Along the coastal zone of the passive margin, since the Miocene,

a series of normal fault footwalls formed topographic highs such as Zanzibar, Pemba and Mafia islands, which further re-routed the main deep-water drainage (Dottore Stagna

—WILEY | 393

et al., 2022). Between 22.9 Ma and 19.8 Ma a submarine landslide of area more than 11,000 km², named the Mafia mega-slide, was emplaced above the reflector M2 (Maselli et al., 2020). The landslide was most likely a consequence of initial volcanism, earthquakes, and drainage changes in the Rukwa-Malawi rift zone, and dynamic uplift of the East African margin in the Western Indian Ocean (e.g. van Wijk et al., 2021).

3 | DATASET AND METHODOLOGY

The two 3D seismic volumes analysed in this study are located offshore Tanzania, in water depths ranging from 600 to 3000 m. The Mafia dataset, to the north, covers an area of 6092 km² of 3D, post-stack Kirchhoff time-migrated, seismic reflection data (Figure 2a). To the south, the Kusini, time-migrated, 3D seismic reflection volume has a total area of 8900 km² (Figure 2a).

For this study, we had access to the first 4.5 seconds (TWT) for both the datasets. The Mafia dataset is characterized by a frequency band spanning from 5 to 115 Hertz. The interval velocities obtained from sonic logs of the two well data vary from 1500 to 2900 m/s suggesting a maximum tuning thickness of 3.2 m down to 24.5 m in the Eocene. The Kusini dataset is instead characterized by a frequency band spanning from 5 to 100 Hertz and an average value of 35 Hertz down to 4.5 seconds (TWT, Eocene). The interval velocities obtained from sonic logs of the two well data vary from 1500 to 2900 m/sec suggesting a maximum tuning thickness of 3.75 m down to 21 m in the Eocene.

3.1 | Well data

Two wells, named Well-1 and Well-2, comprising gamma ray, check shot, velocity and biostratigraphic data, were made available for this study by Royal Dutch Shell and Shell Tanzania. To reconstruct the main chronostratigraphic from the two wells we adopted the biostratigraphy template proposed by Sansom (2018) and Maselli et al. (2020) (Figure 3).

3.2 | Methodology

Seismic and well data were interpreted using Schlumberger Petrel software. We applied conventional seismic stratigraphic interpretation methods as described by Mitchum et al. (1977) as well as attribute analysis to better characterize edge structures. Using the principle of seismic geomorphology, we explored the architecture produced by the edge discontinuities and impedance contrast defining the major sedimentary and structural features.

The chronology of each horizon was estimated through well ties (Figure 3). Synthetic seismic traces derived from the well data were used to calibrate the major reflectors (Figure 3). Horizon M1 (see also Maselli et al., 2020) ties with Well-1 at a true vertical depth below mean sea level (ssTVD) of 2272 m and at below 3505 m ssTVD in Well-2. It dates back to the Priabonian (upper Eocene, Maselli et al., 2020). Horizon M2a (Mid Oligocene) ties above M2 at 2100 m ssTVD in Well-1, which is circa 40–50 m below the Mafia megaslide mapped by Maselli et al. (2020). In the Mafia dataset, horizon M1 usually corresponds to a high-amplitude negative erosive reflection which ties to blocky low values of gamma ray. Horizon M2a instead is marked by a negative reflection, laterally changing in amplitude. Those two horizons (M1 and M2a) were mapped across the two seismic datasets and are used to describe and interpret the Seagap fault zone offshore Mafia Island and Rovuma delta. Although the other two younger horizons were recognized by previous studies in this area (M3 and M4 horizons, Maselli et al., 2020), those are not considered to be fundamental for the scope of the paper because of their strong lateral discontinuity due to erosive channel deposits. Below the M1 horizon, we could not correlate the different seismic units, but we could recognize different seismic packages that will be defined and described when interpreting the seismic lines extracted from the two 3D datasets.

For the Mafia dataset, three surface maps have been realized (M1, M2a and Seafloor) and first two are shown in Figure 4. In the Kusini dataset, we will show surface maps corresponding as a first approximation, to M1 (Figures 11a and 12a,b,c equivalent to the upper Eocene by Maselli et al., 2020), M2 (Figures 11b and 12a,b,c), and the seafloor map (Figure 13). To better trace and map signal discontinuities across the seismic datasets, we used an edge detection attribute known as Dip illumination, which is calculated by illuminating all data points simultaneously, treating each point as lying on a surface described by a reflectance and calculating the local dip and azimuth for each trace. This is a similar approach to that of Chopra and Marfurt (2007). Reflectance can be uniform, if not set to the dip illumination attribute to blend stratigraphic (reflectance) and structural information (azimuth) together. All discontinuities perpendicular to the illumination are enhanced while features parallel to it are attenuated. By rotating the illumination filter and keeping a large area under the illumination, the shaded relief will reveal structure at different orientations resolving different structural details. This attribute has been used
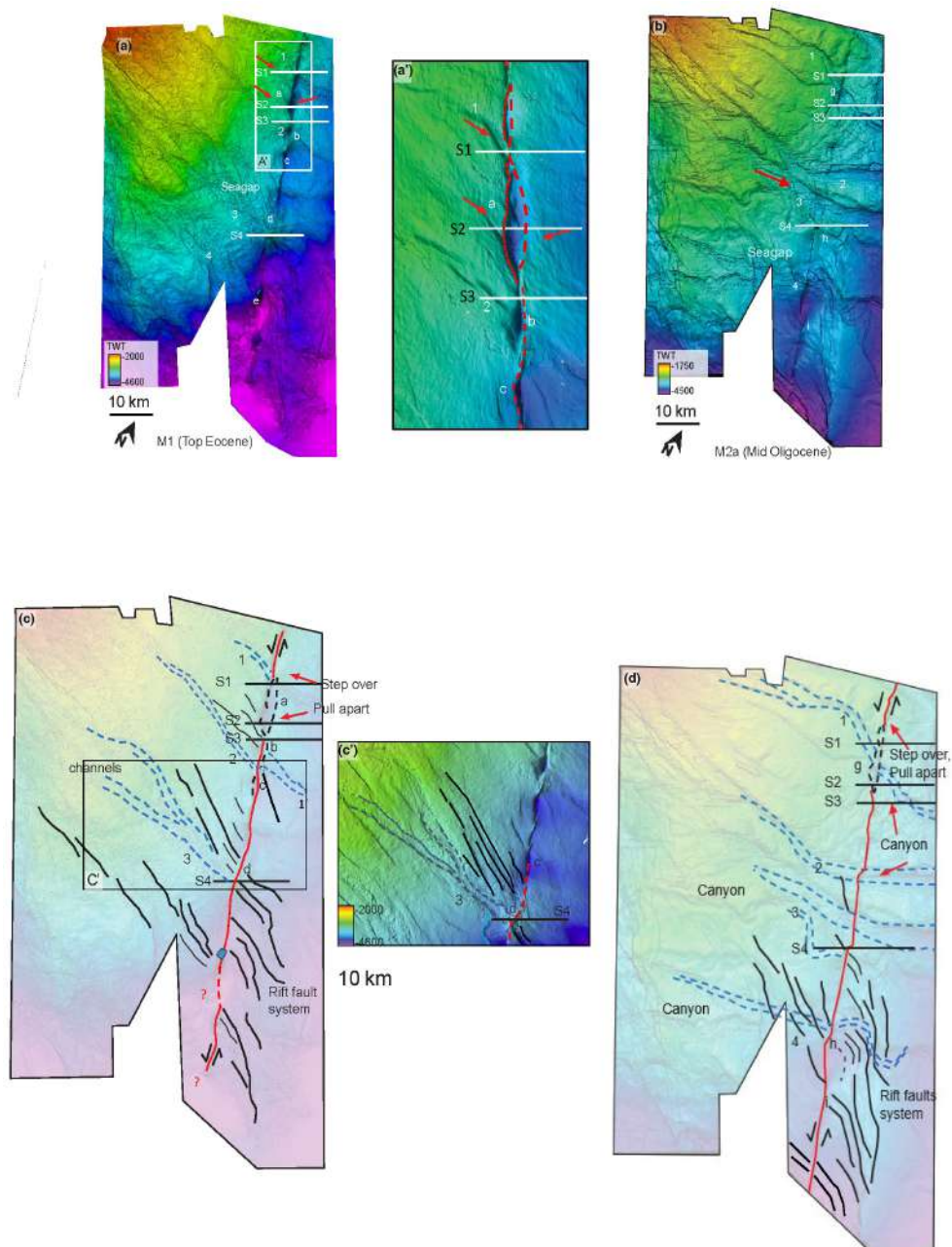
FIGURE 4 Seismic horizon maps from the Mafia 3D dataset. Colour scale bar in TWT. (a) Horizon M1 (top Eocene) showing the seismic geomorphology. 1 to 3 represent the erosive canyons. a to e represent the pull-apart and pop-up structures associated to the Seagap fault zone. (a') details of the pull-apart (a to c) structures. Dotted red lines indicate the Seagap fault (bold) and the relay (thin) fault. (b) Horizon M2a (mid-Oligocene) showing the seismic geomorphology. 1 to 4 represent the erosive canyons. f to i represent the pull-apart and pop-up structures. (c) Interpretative outline of the seismic horizon M1. (d) Interpretative outline of the seismic horizon M2. Red line: Seagap fault zone. Blue dotted line: Erosive canyons. Black lines: Neogene normal faults. S1 to S4 represent the trace of the seismic sections extracted from the 3D Mafia seismic dataset.

to enhance the internal architecture of the Seagap fault zone using time slice data where surface mapping was not available (Figure 9).

Interpreting strike-slip fault systems is often not straight-forward and pitfalls are common, especially when distinguishing structures formed by inversion. Throughout this paper, we have accumulated observations

which geometrically indicate the strike-slip nature of the Seagap fault from the Eocene through much of the Neogene. Some of the key criteria are as follows:

(i) relatively steep faults, often downward steepening
(ii) releasing or restraining bends associated with offsets in the fault trace; pop-ups, pull-aparts

(iii) variable vergence of faults along strike (using low vertical exaggeration sections to distinguish)

(iv) presence of positive or negative flower structures

(v) variable stratigraphy (seismic facies and thickness) across the fault zone (can be confused with inversion)

(vi) timing of deformation

We identify all these criteria in the following analyses in order to determine the nature of the Seagap fault zone in time and space.

4 | RESULTS

Using the 3D and 2D seismic available datasets (Figure 2), the Seagap fault zone can be traced and mapped roughly along a N-S direction across the Kusini and Mafia dataset areas and can be followed to latitude 9°S, beyond which it tips out or is not observable across the available seismic dataset. Towards the southern part of the WSB down to offshore Mozambique, the Seagap fault zone can be projected to the island offshore of Palma (Ilha Rongij, 10°51′S, 40°40′E) where satellite imagery shows a linear feature of the same orientation. Overall, the structure appears to have a length of ca. 400 km.

4.1 | Northern zone, Mafia 3D dataset

### 4.1.1 | Seismic surface map

Two surface horizons tying the two reflectors M1 (top Eocene) and M2a (mid-Oligocene) have been mapped in TWT using the amplitude picking method analysis.

M1: The M1 surface (Figure 4a) deepens from north to south and is affected by several first-order structures and sedimentary features. Some of the major canyons are oriented NW to SE (1–4 in Figure 4a) and are displaced by the large N-S to NNE–SSW-oriented fault structure, and a series of faults oriented NW-SE, displacing or bordering the main erosive canyon. The longest and largest visible N-S to NNE–SSW structure it the Seagap fault zone. Along its trace, the fault shows clear bending and offsets around topographic uplifts (d and e in Figure 4a) and topographic depressions (a, b, c in Figure 4a,a′,c), defining pop-up structures and pull-apart basins respectively. Where left-lateral strike-slip faults are left-stepping, the region of overlap is in tension, resulting in pull aparts. When the geometry is reversed, the offsets are right-stepping, and the region between offsets is in compression leading to pop-up structures. These pop-ups, as well as pull-apart structures, are diagnostic of strike-slip

faulting (e.g. Aydin & Nur, 1985). The small pull-apart basins in Figure 4a′,c′ show steepened edges bordering to the east side of the Seagap fault trace, while the pull apart b appears mirrored with respect to the others. In d and e (Figure 4a), we observe instead the presence of a contractional bend around an antiformal structure. In e, we also observe a clear extrusive feature intruding on the antiformal structure (Figure 4a). Across the surface, we mapped two major erosive canyon-like features (1–2 in Figure 4a,c,c′) oriented NW-SE and variably affected or interrupted by the Seagap fault (Figure 4a,c). Canyon 1 is interrupted by the Seagap fault as shown in Figure 4a,a′. In annotated Figure 4c, Canyon 1 is visible on the left side of the Seagap but is absent on the right side where instead an erosive feature is observed. Canyon 3 which is the better-preserved erosive feature, shows a bifurcating geometry and is similarly interrupted against by restraining bend structure d as clearly shown in the magnified Figure 4c′.

M2a: The M2a surface (Figure 4b) roughly corresponds to the Rupelian–Chattian (mid-Oligocene) interval. Similar to the M1 surface, the first-order features are represented by WNW-ESE major canyon type erosive features (1–4) affected by NW-SE faulting. The fault trace bends around two main pull aparts (f and g) and the restraining bend structure (h). Four main canyons appear variably affected by the Seagap fault (Figure 4b). The first canyon (1), with bifurcating and meandering architecture (Figure 4b) is left laterally offset by the Seagap fault with the west side deformed by the pull-apart basin and the east side showing the bed width enlarged and preferentially eroding the east bank (Figure 4d). The erosive canyon features 2 and 3 appear instead to erode the Seagap fault zone (Figure 4b), apparently (at a seismic scale) unaffected by the strike-slip displacement. Channel 2 appears also to have eroded an older lateral meandering channel (3, Figure 4b). The two erosive features are also further deformed by the NW-SE normal fault (red arrow Figure 4b). The fourth canyon (4) is instead slightly offset (left lateral) and interrupted by the topographic high (h Figure 4b) and the following pull-apart structure (i Figure 4b).

The relationship between the structural effect of the Seagap fault zone and the major sedimentary features from Late Eocene through the Middle Oligocene (see Maselli et al., 2020 for details on the ages), is given in Figure 4c,c′,d. These three schematics show the major normal fault network (bold black line) and erosive canyons mapped (blue dotted) with respect to the Seagap fault (red). In Figure 4c, corresponding to the top Eocene event, the Seagap fault appears to clearly interrupt the main erosive canyon structure and to cut through the
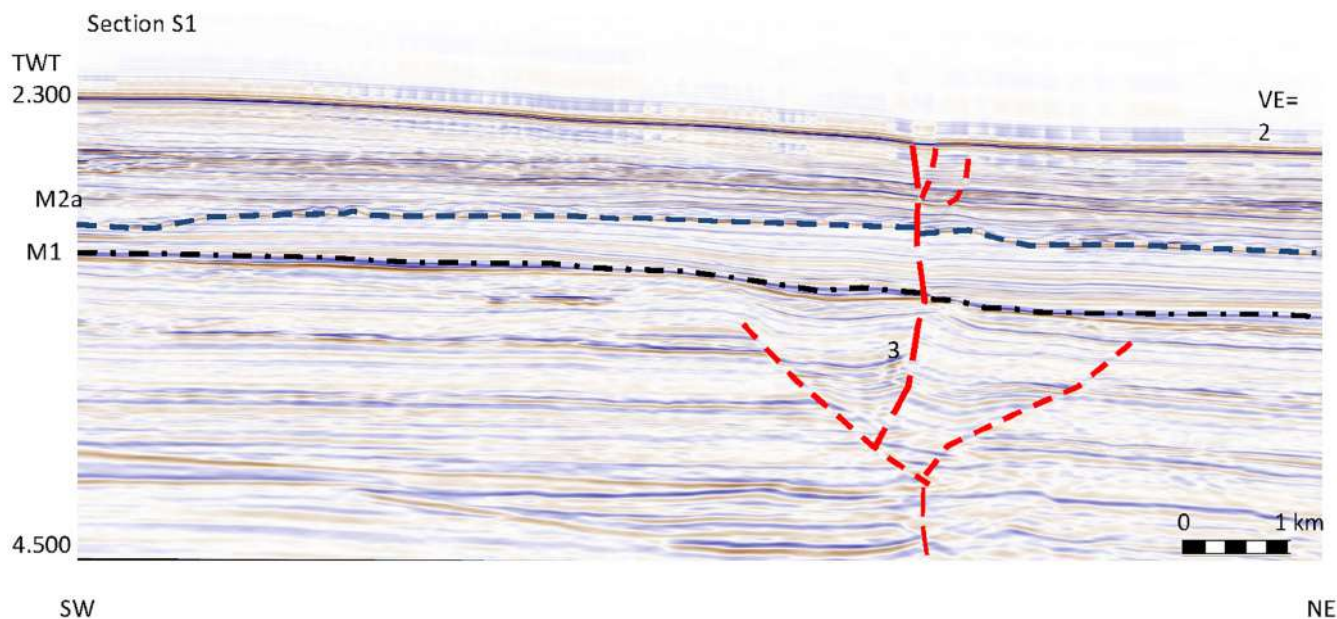
FIGURE 5 Interpreted seismic section S1 extracted from the 3D Mafia dataset showing the Seagap fault zone. Bold red dashed line: The Seagap fault zone. Red dashed line: Extensional fault. Black dotted: M1 horizon. Blue dashed line: M2a horizon. VE = 2.

NW-SE oriented major normal fault. In Figure 4d (surface M2a—mid-Oligocene), in contrast to M1, the two channels (2 and 3) appear not to be displaced by the Seagap fault except for the first and fourth canyons, which suggest a left-lateral displacement. In Figure 4d, the NW-SE extensional fault appears to reorient and offset the channel 4 with an apparent left lateral shear sense.

4.2 | Seismic interpretations

To characterize the deformation across the releasing and restraining bend structures related to the Seagap fault, we interpreted four seismic sections (S1 to S4) cutting, respectively, the releasing and the restraining bend. All the seismic sections presented are in TWT and are shown with a vertical exaggeration of 2. The main reflectors mapped for reference are M1 and M2a, as discussed above. The black dotted reflector E represents a regional erosive feature.

4.2.1 | Seismic section S1 (Figure 5)

This seismic section crosses the Seagap fault in an area devoid of synformal morphology above M1. This is clearly shown by the seismic data that images a structural feature below M1, we interpret to be a negative flower structure where the major vertical fault strand (bold red dotted) shows a minimal normal displacement component (M2a

and M1). Below M1 this fault appears to juxtapose units of different seismic stratigraphy, suggesting an important N-S oriented strike-slip component. This structure is interpreted to be the Seagap fault, indicating its significant strike-slip character.

4.2.2 | Seismic section S2 (Figure 6)

The section transects a structural low (releasing bend) as shown in Figure 4a, which images a synformal structure deformed by a conjugate extensional fault system. Below M1 the seismic packages are characterized by high-frequency parallel-continuous reflectors while above the M2a reflector the seismic packages are characterized by an alternation of chaotic units, with layered units, overlain up to the seafloor by a seismically transparent unit, interpreted by Maselli et al. (2020) as a regionally important mass-transport deposit. Fault 1, which with faults 2 and 4 are part of the offshore extensional rift (Figure 2), represents an extensional fault that tips out between M1 and M2a. Fault 2 appears as a high-angle structure (section oblique to their direction) with a reverse displacement (see the dotted pale blue reflector) affecting the seafloor. Fault 3 is a high-angle extensional fault affecting the entire seismic package to the seafloor. The fourth fault (4) represents an apparent low-angle normal fault, although its orientation is oblique to the transect. This fault does not affect the seafloor. It should be noted that fault 3 in this section 2 dips to the east while its corresponding fault in section 1 is sub-vertical.
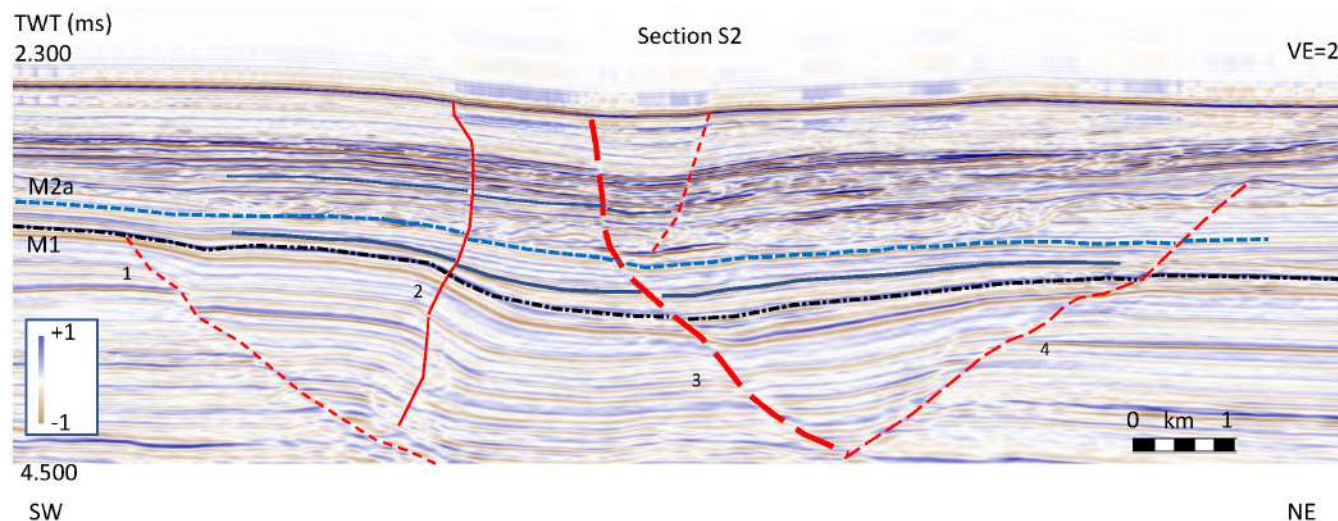
FIGURE 6 Interpreted seismic section S2 extracted from the 3D Mafia dataset showing the Seagap structure across the pull apart structure b (Figure 4). Bold red dashed line: The Seagap fault. Red dashed line: Extensional fault. Black dotted line: M1 horizon. Blue dashed line: M2a horizon.
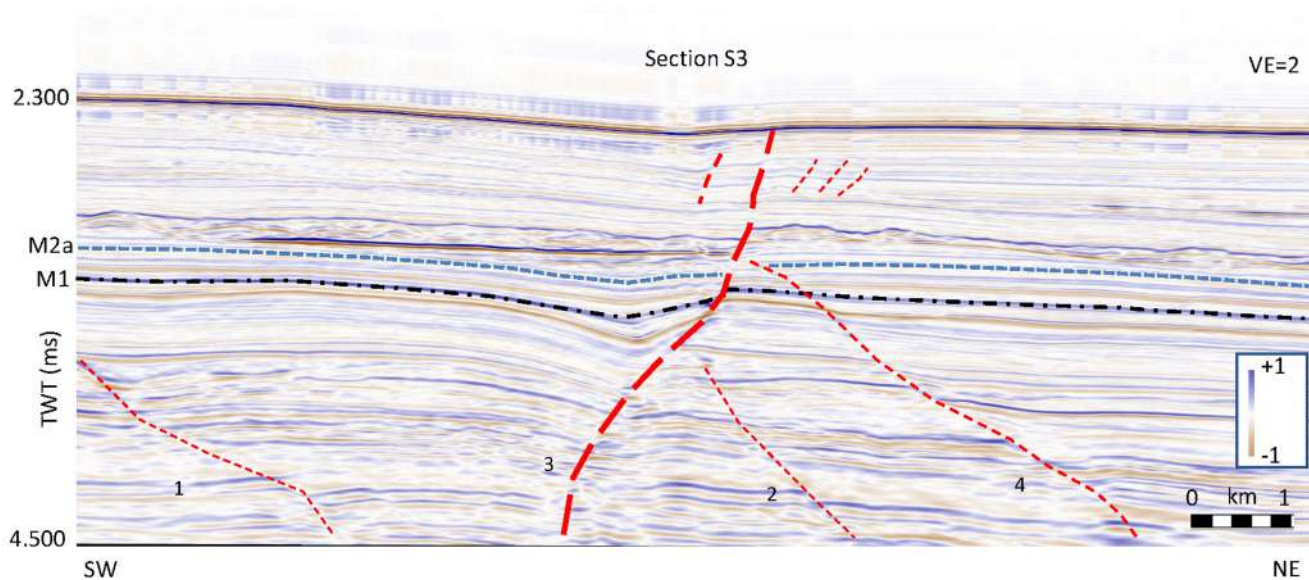

FIGURE 7 Interpreted seismic section S3 extracted from the 3D Mafia dataset showing the Seagap flower structure between the pull-apart structure b and c (Figure 4). Bold red dashed line: the Seagap fault. Red dashed line: Extensional fault. Black dotted line: M1 horizon. Blue dashed line: M2a horizon.
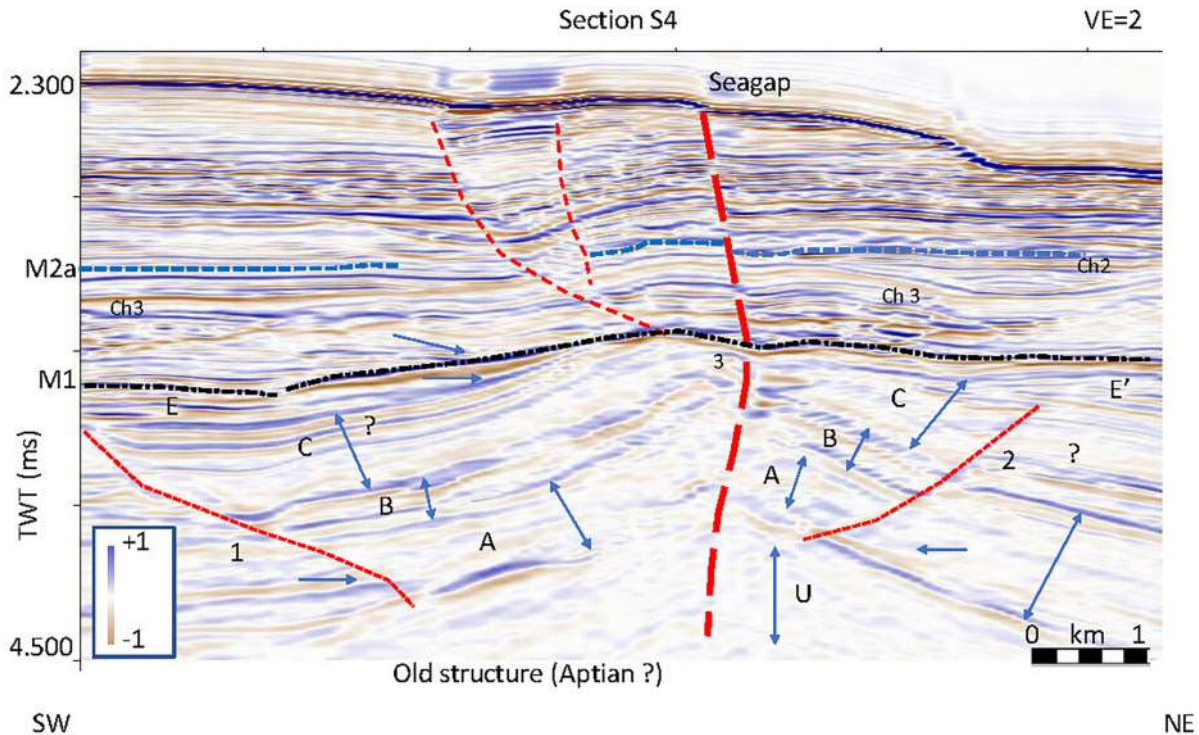
4.2.3 | Seismic section S3 (Figure 7)

This seismic section is extracted from the 3D Mafia dataset and represents a transect cutting across the north part of the releasing bend a in Figure 4. The section shows a major steep fault (fault 3, bold red dotted) which displaces the major units (the MTD above M2a, the reflector M1) with normal offset of approximately 0.2 second TWT. This fault represents the Seagap fault zone. In the hanging wall, the reflector M1 shows a

small synform representing the north side of the releasing bend b. West (hanging wall) and east (footwall) of this fault, we observe three normal faults (1, 2 and 4) which are offsetting units older than M2a (red arrows Figure 4a,a′). Fault 1 is shown in Figure 4a′ by the red arrow. Those faults relate to the NW to SE extensional structures affecting the offshore Tanzania rift (Maselli et al., 2019). This is a classic stepover geometry where fault 3 on section S2 is now in Section 3 accommodating deformation along the trace of the Seagap system with a

FIGURE 8 Interpreted seismic section S4 extracted from the 3D Mafia dataset showing the Seagap fault zone across the restraining bend d (Figure 4). Bold red dashed line: The Seagap fault. Red dashed line: Extensional fault. Black dotted line: M1 horizon. Blue dashed line: M2a horizon.

very steep west dip. This overall left-stepping geometry has created the pull-apart synformal structure observed on these two lines.

4.2.4 | Seismic section S4 (Figure 8)

The fourth 2D seismic section (extracted from the 3D Mafia dataset) is shown in Figure 8 and intersects a zone of high structural complexity, interpreted to be a restraining bend structure (d in Figure 4a,b). Two main seismic packages can be recognized: (a) above the black dotted erosive horizon M1, a seismic package characterized by layered and channelized seismic sub units mainly affected by fault with an extensional component; (b) below horizon M1, which includes four seismic sub-packages (U, A, B and C) characterized by transparent seismic facies (U, A, C) and a thick layered and reflective unit (B) all of which are deformed into an apparent antiformal geometry by three major faults. The near-vertical Seagap fault (red dotted thick fault) with a slight bend upward, divides the entire pre-E package into two boundary fault blocks showing opposing dips. The deeper seismic packages U, A, B, C can be recognized on both sidewalls, but their relative thickness variations suggest a pre-Seagap fault depositional and structural history. The two last

sub-packages (E and E′), below the horizon M1, show different seismic facies across the two fault blocks and are characterized by reflectors onlapping on the top C subunit towards the fold hinge zone. Seismic package C shows similar facies on both fault blocks but with different lateral thickening. The reflective package B, concordant with the C and A packages, appears correlated across both fault blocks. The sub-package A shows similar seismic facies on both fault blocks and is instead layered with the low internal reflectors onlapping to the basal boundary (again towards the hinge zones). The deeper sub-package U shows a very low amplitude, chaotic character that does not allow recognition of the internal seismic stratigraphy but still shows the antiformal structure. The apparent low-angle extensional faults 1 and 2 are confined below horizon M1 and are affecting the folded fault blocks by displacing the A, B, C packages. The M1 horizon is clearly eroding both the E and E′ packages and cutting the chevron folding of the pre-E packages, suggesting a pre-erosive structural event. Within the upper package, above the E erosive feature the reflectors are onlapping. The seismic unit included between package E and reflector M2a shows a complex seismic facies distribution defined by channelized structure (Ch1-Ch3) eroding layered seismic units. Above M1, the Seagap fault appears to change kinematic styles exhibiting a

FIGURE 9 Time slice from the 3D Kusini dataset showing dip illumination attribute. (a) Time slice at 4.4 TWT second; (b) time slice at 3.3 sec in TWT second. Red line. Seagap fault trace. Red dotted: Secondary extensional faults. S5 and S6: Trace of the 2D seismic lines extracted from the 3D dataset. Black box: Restraining bend structure (see Figure 11).
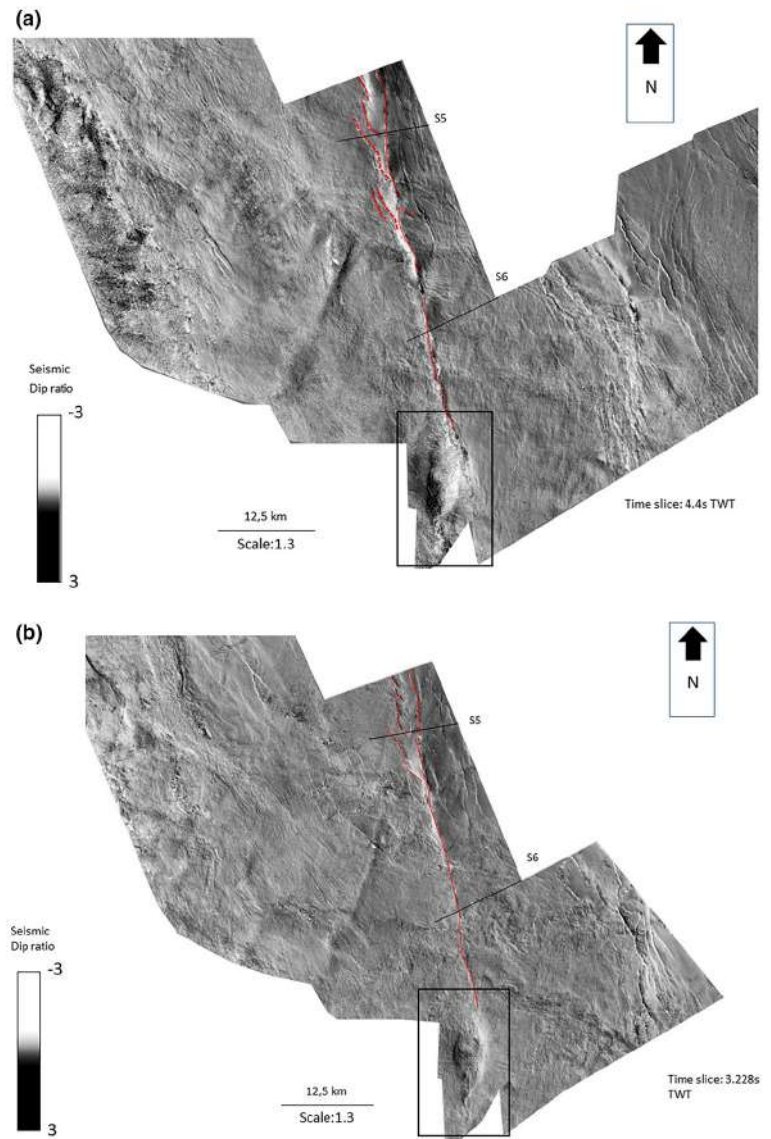
normal fault displacement. The two extensional faults (red dotted) affecting the entire package 1 suggest, like the Seagap fault, they too have accommodated recent tectonic activity.

4.3 | Southern zone, Kusini 3D dataset

The Kusini dataset is located south of the Mafia 3D dataset and the Block 2 area (Figure 2). However, due to the highly erosive canyon activity, it is difficult to map continuously the M1 and M2 equivalent horizons. Therefore, we could not produce a reliable continuous surface across the entire block dataset, and instead used time slices extracted from a dip illumination 3D attributes volume. We concentrate on mapping horizons M1 and M2 in two specific areas across the restraining bend produced by the southern continuation of the Seagap fault (Figure 11)

4.3.1 | Dip illumination data and seismic sections (Figures 9 and 10)

Dip illumination maps (Figure 9a,b) effectively highlight both subtle and major edge structures. Given the southeast deepening of the seafloor, the two time slices are taken from sections at 4.2 TWT and 3.2 second TWT. In both images (Figure 9a,b), the Seagap fault appears to be present throughout almost the entire dataset south to the restraining bend structure (black box Figure 9) where our dataset ends.

The deeper time slice at 4.2 sec (Figure 9a) and vertical seismic sections in Figure 10a,b at approximately the depth of the M1 horizon, delineate the Seagap fault geometry across the deepest seismic unit package (Eocene-Miocene). The fault trace is relatively straight and characterized by different fault segments with secondary associated faults (red dashed fault Figure 9). Figure 10a shows the seismic section S5 crossing the Seagap fault zone with location in
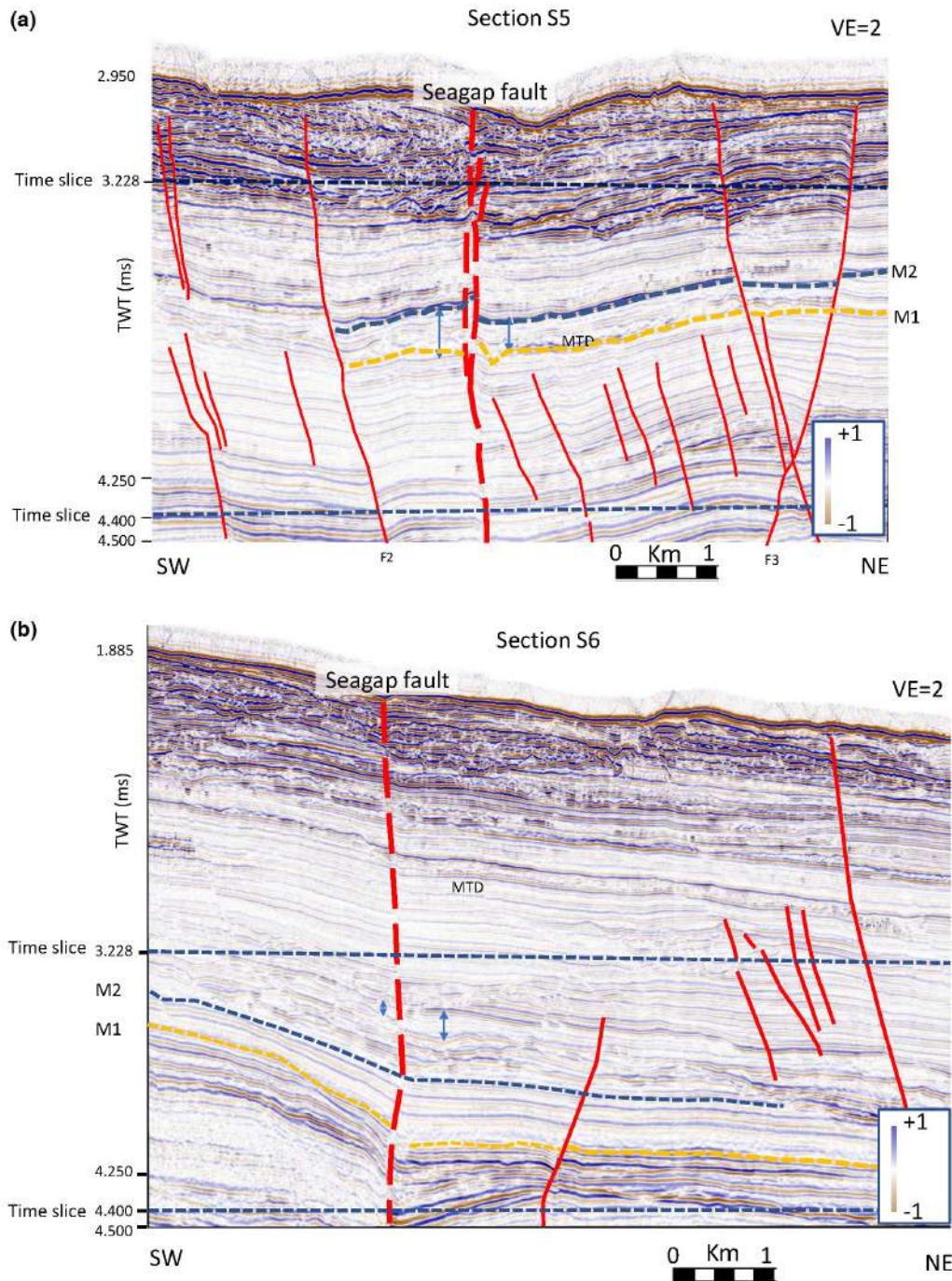
FIGURE 10 Interpreted seismic sections S5 and S6. Extracted from the 3D Kusini dataset showing the Seagap structure (Figure 9). (a) Seismic section S5. (b) Seismic section S6. Bold red dashed line: The Seagap fault. Red dashed line: Extensional Neogene fault. Orange line: M1 horizon. Blue dotted line: M2 horizon. Horizontal dotted line: Trace of the time slice shown in Figure 9.

Figure 9, and secondary associated high angle structures. Displacement recorded by the deepest units (Eo-Miocene?) highlights the normal nature of the high-angle associated faults. The hanging wall of F2 and footwall of F3 appear gently folded below the 4.2 sec TWT. Above 4.2 sec, the fault F2 appears to behave as a high-angle normal fault. The same can be observed across fault F3. The Seagap fault is the main structure observed across the seismic section S5 and S6 and appears to juxtapose fault blocks with no lateral continuity of seismic reflectors across the fault, indicating a transcurrent offset. In Figure 9b, we do observe a shallower time slice (3.2 TWT) with fault structure more continuous than the deeper slice along strike. The fault still ends before the restraining bend highlighted by the black box. This time slice on both the right and left fault blocks shows less but more distinctive fracture.

FIGURE 11 Mapped seismic horizon from Kusini 3D data set (location in Figure 9). (a) Seismic horizon M1 (b) Seismic horizon M2. Traces from S7 to S9 represent the seismic sections in Figure 12.
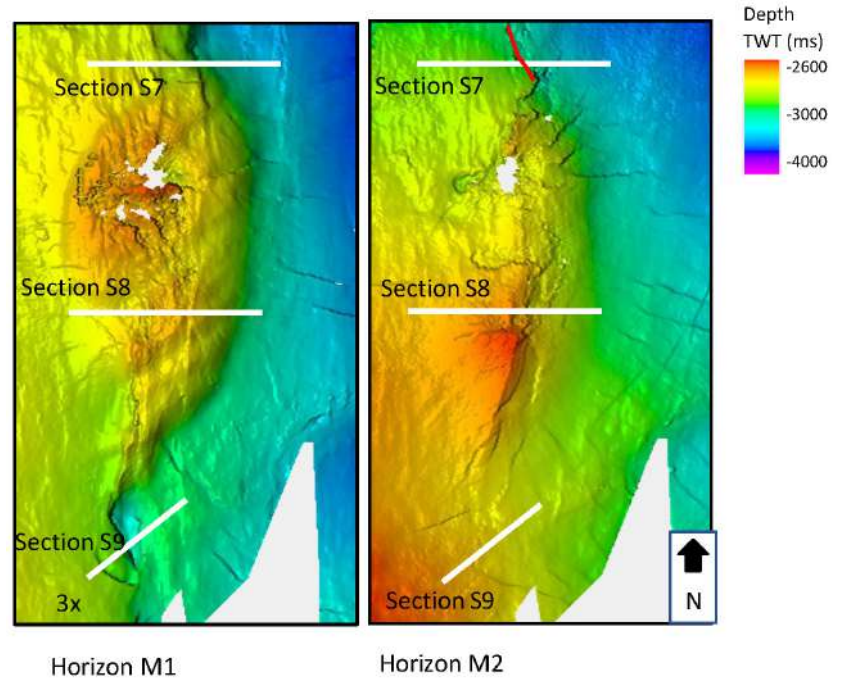

Horizon M1   Horizon M2

Figure 10a shows the seismic section across the north part of the Kusini dataset, crossing the Seagap fault. It images the complex structure of the Seagap fault defined by different high-angle faults that bifurcate upward and offset the entire seismic section from the seabed down to the deepest upper Eocene units. The Seagap fault juxtaposes two fault blocks showing slightly different seismic stratigraphy and thickness. Figure 10a shows the extensional nature of the deformation surrounding the Seagap fault. Figure 10b shows a southern section of the Seagap fault. The fault appears more continuous with fewer secondary faults, and is generally a single discontinuity affecting the top Eocene to seabed. Again, the two blocks separated by the Seagap fault do not reflect symmetrical thickness and stratigraphy of the same seismic units suggesting, along with the structure's steepness, the transcurrent nature of the fault.

4.3.2 | Restraining bend structure (Figure 11)

In Figure 11, we explore the restraining bend structure representative of the Seagap fault (Figure 11a,b). The structure is characterized by high topographic elevation and is coupled to a small releasing bend (along section S7).

Horizon M1

The surface map of horizon M1 (orange reflection in Figure 12) illustrates the architecture of the restraining bend where the Seagap fault appears to change orientation (the bold red fault). The restraining bend is characterized by an antiformal structure affected by normal and transtensional faults and the surrounding radial fractures. The

gap on the surface represents the area where the green horizon is strongly eroded and therefore poorly mapped. The restraining bend transitions southward into a releasing bend defining a small basin bounded by an east-dipping normal fault.

Horizon M2

The surface map of horizon M2 (purple reflection in Figure 12) still shows similar structural characteristics as M1. An antiformal structure represents a topographic high with surrounding associated secondary extensional faults. At this time horizon, the releasing bend basin is not imaged and appears filled and draped by units including the purple reflector.

On both surfaces, the Seagap fault does not cut through either the antiformal structure or the extensional basin defined by the releasing bend.

Seismic section 7 (Figure 12a)

This seismic section crosses the southern termination of the Seagap fault (still visible as by dotted red line) which is deformed and further displaced by late west-dipping normal faults. From older to younger the main seismic units are represented by:

- Seismic package 4 contains an anticlinal geometry and is characterized by layered and transparent seismic facies. The top of the seismic package is defined by the yellow reflector partly eroded by the black dotted unconformity, and on both flanks onlapped by the seismic layers of the seismic package 3. The package is clearly cut by the Seagap fault zone.
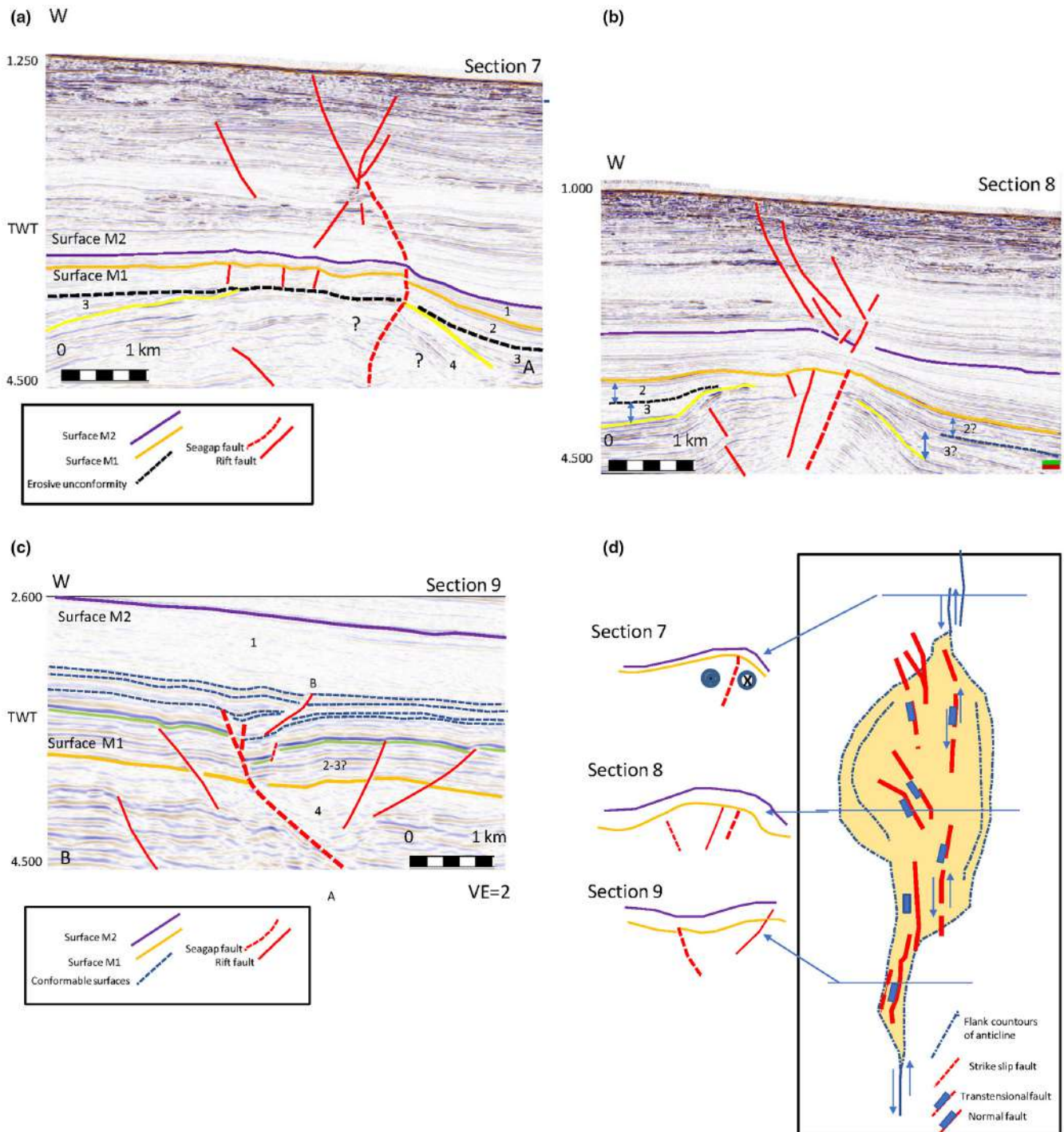
FIGURE 12 Interpreted seismic sections S7 to S9, TWT. (a) Interpreted seismic section S7, showing the Seagap structure. (b) Interpreted seismic section S8, showing the Seagap structure. (c) Interpreted seismic section S9, showing the Seagap structure. (d) Sketch of the restraining bend with outline of the Seagap fault architecture from S7 to S9. Orange line: M1. Purple line: M2. Blue dotted line: Conformable unit. Black dotted line: Unconformity. Red dotted line; Seagap fault.

- Seismic package 3 asymmetrically onlaps the underlying anticlinal structure and shows lateral thickening on both flanks of the anticline, suggesting a syntectonic depositional relation with the anticline. Seismic unit 3 is eroded by the black dotted unconformity, which is older than the horizon M1.

- Seismic package 2 is defined by a transparent seismic unit draping the unconformity and is offset by a vertical structural discontinuity.

- Seismic package 1 drapes unit 2 but shows a lateral thickening along the east flank of the antiform, suggesting a late reactivation of the east flank structure of the

antiform. Above the package 1 (M2) the seismic shows a series of depositional units with a similar post-Miocene history to the Mafia area.

The deformed geometry reflects the reactivated nature of the Seagap fault. The asymmetric distribution with respect to the Seagap fault and the lateral thickening nature of the package 2 point to a previous syn-tectonic origin of the now reworked package 4 as an antiformal structure. The overlying post-surface 2 unit is affected by extensional structures which further displace the still active Seagap fault.

Seismic section 8 (Figure 12b)

This seismic section crosses the central portion of the main restraining bend. From bottom to top it shows a well-developed antiformal structure (up to the yellow reflection) affected by high-angle faults with a normal component. Where heavily faulted, the core of the antiformal structure is seismically incoherent, reducing our capability to map and correlate the internal reflections. A vertical structure affecting the entire subsurface is not observed, suggesting that the Seagap fault does not cut through the entire section. Similar to what is observed in Figure 12a, seismic packages 2 and 3 asymmetrically onlap the two flanks of the antiformal structure. The seismic facies and relative thickness characterizing those two packages are quite distinctive on both flanks of the antiform: a transparent and thinner seismic unit on the west flank and a thicker, more strongly layered facies on the east flank. This suggests the Seagap fault must have a transcurrent component juxtaposing the two flanks of the antiformal core soon after the yellow surface erosion. Above the M1 and below M2, we can map a laterally continuous seismic package draping the main antiform, suggesting that by that time the main fault activities had ceased. Above, similarly to what was observed in the lateral section in Figure 10a, we observe the presence of conjugate and extensional faults deforming the late Neogene units.

Seismic section 9 (Figure 12c)

Seismic section 9 represents a section across the associated releasing bend along the Seagap fault. The section shows a thicker unit 1 than section 8 and is devoid of the unconformity dividing seismic packages 2 and 3 which now are merged into a single composite seismic unit for simplicity.

The lower unit is characterized by package 4 which shows more complex internal seismic facies (layered to transparent subunits) and is offset by a primary extensional structure with a large normal component (A) representing the Seagap fault. Its hanging wall rollover contains both packages 2 and 3, and a secondary antithetic normal fault. Horizon M1 is clearly displaced by the extensional fault, which creates an extensional basin containing packages 2

and 4. No through-going vertical structure offsets the basin suggesting the Seagap fault is no longer active in the releasing bend.

Below M2, we observe a thicker package than is observed in the previous two northern sections, indicating a thickening of this seismic unit towards south. The lower part of this unit is characterized by a series of seismic units (dotted blue reflectors) draping on M1 but still affected by the normal faults A and the west dipping younger normal fault B. The upper part of this package appears unaffected by deformation.

In Figure 12d, we outline a simple sketch summarizing the internal structures mapped across the restraining-releasing bend structures. The sketch shows the restraining bend is unaffected by a high angle transcurrent fault, but part of the strike-slip component of the Seagap fault zone is instead absorbed by the secondary extensional faults. The deformation shows a slight younging towards the south.

4.4 | Seafloor structure

The seafloor structures are visible on the surface maps in Figure 13. Both surfaces show the Seagap fault cutting the seafloor but with no visible active strike-slipcomponent.

4.4.1 | Mafia area seafloor

The Mafia seafloor seismic surface shows large-scale structural and depositional features affecting the slope basin structure. We can observe three main erosive gullies (a to c) eroding down towards east which are cutting through the Seagap fault (white arrows). On the west side of the seafloor map, a N-S meandering channel is observed as well as an older straight canyon (d) which appears beheaded by the Seagap fault trace.

4.4.2 | Kusini seafloor

The Kusini seafloor seismic surface appears much more complex. It represents the seafloor of a slope basin structure affected by much more erosive structures: major channels eroding down slope and several small gullies some of which clearly triggered from the lower slope. The Seagap fault (white arrows) deforms the seafloor although its edges are barely seismically visible and do not show any visible active strike slip component displacement affecting the erosive features (canyon and gullies). Down the slope structure on the southwest portion of the surface map several active normal faults
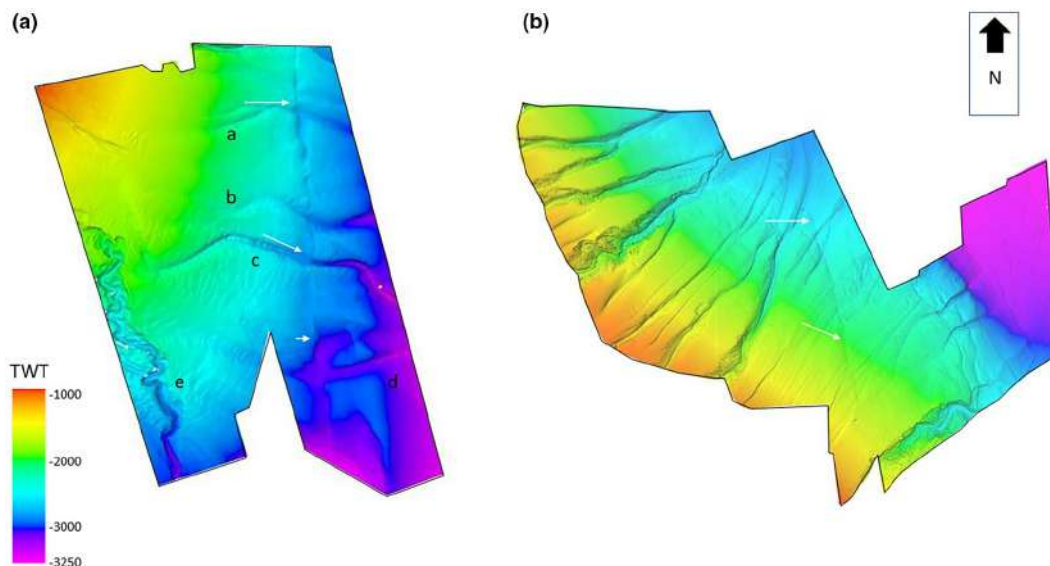
FIGURE 13 Seafloor seismic map. Colour scalebar in TWT. (a) Seafloor mapped from the Mafia 3D dataset. A to c represent the main erosive canyon. (b) Seafloor mapped from the Kusini 3D dataset.
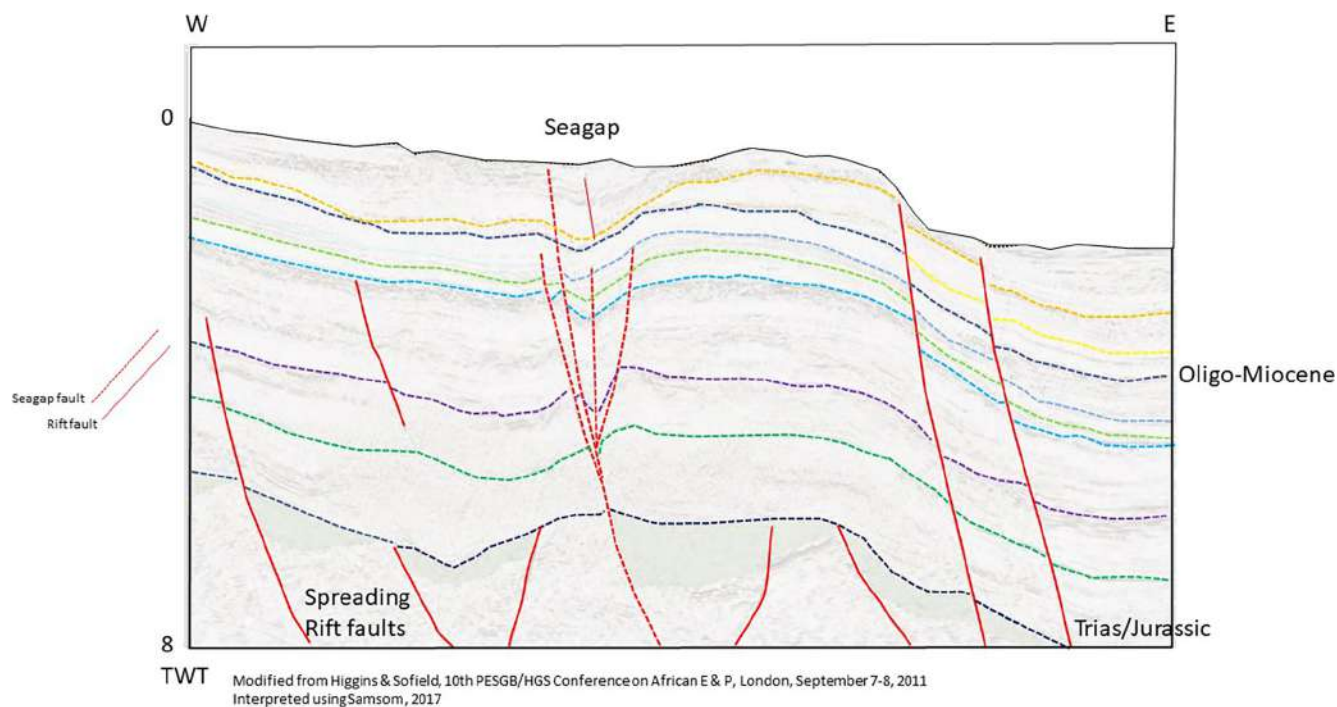

FIGURE 14 Line drawing of the ION geophysics 2D section extracted from ION TZ-2700 obtained from Higgins & Sofield, 10th PESGB/HGS conference on African E & P, London, September 7–8, 2011 and located in Figure 1, using Rego et al. (2019). Line drawing interpreted using Sansom (2018) horizon maps.

deform the seafloor with no evidence for a strike slip component.

Overall, the Seagap fault seems to lack the clear and visible strike-slip kinematic component that has characterized the Eocene to Miocene units in favour of a normal fault style of deformation. The seismic sections in Figure 10a,b (but also Figures 6 to 8 from the Mafia dataset) both show that above 3.2 TWT section the Seagap fault acts a predominantly as a normal displacement fault.

4.5 | Deep section (Figure 14)

The main limitation of the seismic data utilized in this research is the lack of information below 4.2 sec

TWT. However, we have interpreted the Higgins and Sofield (2011) deep seismic section cutting across the offshore Tanzania basin (the exact location is not published). We interpreted it using the stratigraphic framework proposed by Sansom (2018) for the seismic units older than the Eocene. The modified section is represented in Figure 14 and shows the seismic data down to 8 sec TWT, crossing the Seagap fault. The Seagap fault (red dotted line) appears as a negative flower structure rooting into and reactivating a deep pre-existing Jurassic transform fault formed near the ocean-continent transition offshore Tanzania. This transform formed as Madagascar separated from Africa, and it is a structure apparently co-eval with the Davie Ridge. It coexists with seismically active normal faults which affected the entire offshore basin during the late Neogene, as systematically observed across our previously described seismic sections and horizon maps. A similar relationship of the Seagap fault to Jurassic rift faults is also observed in ION T23 proposal by Rego et al. (2019). The breadth of the deforming zone within the oceanic lithosphere remains debated, with diffuse deformation between the coast and northeastern Madagascar, inferred from models of GNSS data on the mainland and Madagascar (Stamps et al., 2020). Our studies suggest that some of that strain is partitioned along the Seagap fault zone.

5 | DISCUSSION

### 5.1 | Seagap architecture and strike slip reactivation structures

Within this still incompletely understood regional crustal context, the Seagap fault zone is an enigmatic structure as many uncertainties remain regarding its structural evolution with respect to both its reactivation during Oligocene-Recent East African rift activity and the Davie Ridge uplift. Rego et al. (2019) describe the Seagap as a sinistral transcurrent fault whose structural culminations control location of the main aligned traps of Aptian to Eocene age reservoirs. Sansom (2018) shows additional coherency slices supporting the late Oligocene sinistral strike slip configuration, describing convoluted channel patterns, and the amalgamation of a few input channels into major trunk systems of mid-Campanian to base Tertiary age, all of which are sinistrally deflected by the Seagap fault. Our study confirms active sinistral kinematics certainly until the Plio-Pleistocene? time. Furthermore, we support the concept already proposed by Phethean et al. (2016), Rego et al. (2019) and Roche and Ringenbach (2022) that the Seagap is an old regional structure (at least pre-Aptian), which we have interpreted as active since the late Eocene

time as transcurrent structure but only recently (late Pliocene to Pleistocene to nowaday?) reactivated as a normal fault structure. What remains debated is whether the ocean-continent transition lies west or east of the Seagap fault, and our results provide no new constraints.

The few available deep seismic data we could access from the literature (Higgins & Sofield, 2011; Roche & Ringenbach, 2022; Sinha et al., 2019) (see Figure 14) suggest that the Seagap fault did re-activate deep transform structures of Late Jurassic age that formed as Madagascar rifted from Africa. A new catalogue of earthquakes of M > 4 during the time period 1900–2020 reveals a ca. 100-km-wide zone of seismicity from the Tanzania and Mozambique and spanning the Seagap and Davie Ridge. Focal mechanisms for the larger instrumentally recorded earthquakes reveal primarily normal faulting along N-S planes, with some NNW–SSE strike-slip mechanisms (Figure 2b), indicating that the strike-slip fault systems are now accommodating E-W extension. This is in agreement with the regional stress field previously proposed by Delvaux and Barth (2010) and Craig et al. (2011) and our seafloor structural observation (Figure 13). This pattern of strain is in contrast to the Comoros volcanic chain where both ca. E-W extension and N-S opening along E-W striking planes are observed, and a leaky transform has been interpreted (e.g. Bertil et al., 2021). The general lack of Neogene-Recent magmatism along the Seagap fault system contrasts with the Comoros ridge, and the Davie Ridge south −14°S, where sills, dikes and extrusive lavas are found (e.g. Courgeon et al., 2018).

The relatively shallow seismic lines presented in section S1 (Figure 5) to S5 (Figures 5–8), support the interpretation of ongoing extension along the Seagap fault zone. Figure 5 (section S1) and 6 (section S2) show the Seagap fault bordering and crossing a releasing bend and still acting as a normal fault. Across the restraining bend (Figure 8) the Seagap fault appears to create more complex structures but all the most recent deformation appears to be extensional. All sections in Figures 5–8 (Mafia dataset) and Figures 10 and 12 (Kusini dataset) allow us to infer a four-stage evolution of the fault as proposed in the simple sketch in Figure 16.

Some initial transtensional structures, shown diagramatically in Figure 16 as a horst although could involve earlier faults, were inverted creating antiformal structures (inversion stage, Figure 16). After a period of relative quiescence, the pre-existing faults were reactivated as a strike-slip structure (strike-slip reactivation phase, Figure 16). An indication of what could have been the local pre-Neogene basin architecture before the Seagap fault reactivation can be unravelled from the seismic section 9 (Figure 12c,d) at the releasing bend south of the Kusini dataset. In that pull-apart basin, the Seagap
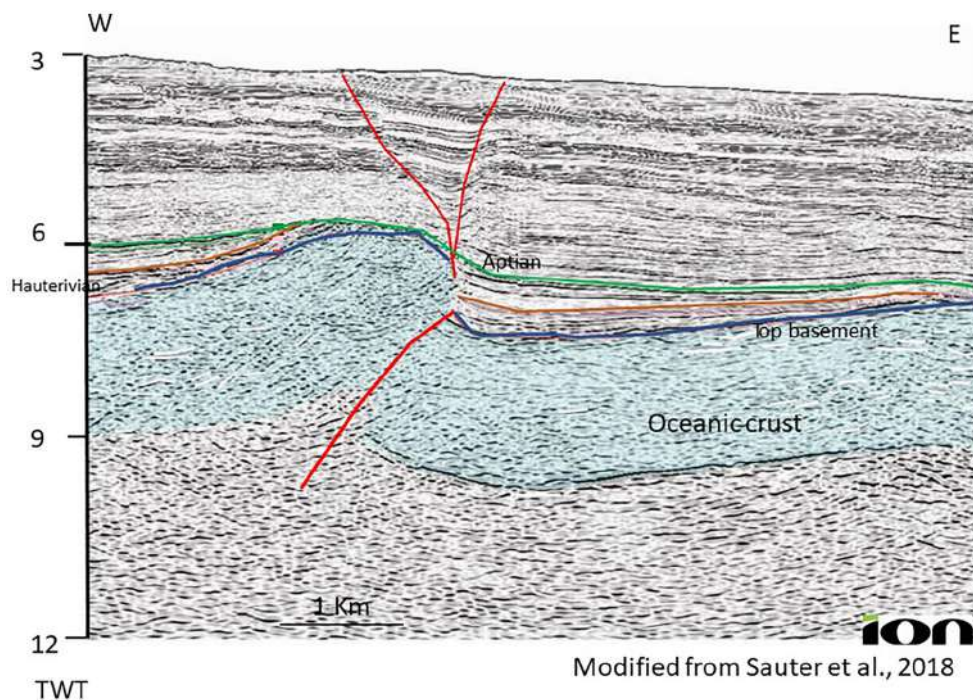
FIGURE 15 Seismic reflection profile (modified from Sauter et al., 2018), interpretation illustrating thrusting and buckling of the oceanic crust. Note that the Aptian horizon lies directly on the top basement high centred at 6 TWT indicating an erosion phase that has removed Hauterivian and earlier layers after the thrusting. Seismic trace is located in Figure 1.Vertical exaggeration: ca. 1×. Courtesy of ION geophysical.

fault zone affects the basin and the main pre-Eocene depositional structure as a normal fault, essentially creating a graben filled by synrift deposits (e.g. lateral thickening seismic packages 2–3, section 9) within a hanging wall roll over. Similar architecture pre-strike slip deformation is proposed by Sadiki et al. (2021) in their analogue experiment. Therefore, those sections allow us to propose a possible scenario across the releasing bend structure as shown in Figure 16. The initial pre to synrift extensional units (Late Jurassic stage, named Transtensional stage in Figure 16) which are not entirely visible and therefore are inferred from our seismic section (S9) and the literature (Sauter et al., 2018), were reactivated within a restraining bend to produce pop up or inverted structures (see Figure 12; Upper Cretaceous inversion stage Figure 16). Those structures are apparently onlapped by laterally thickening units and then drastically eroded since the Eocene (passive margin stage, Figure 16), producing the dismembered pop-up structures observed on the seismic sections S7 and S8. Although not the focus of this paper, it is worth noting that in several cases, those transpressional structures are later intruded by over pressured fluid as fluid pipe structure or mud volcanoes (Rego et al., 2019; see the intrusive feature f in the surfaces in Figure 4a,b). Sadiki et al. (2021) modelled a very similar scenario in the Block 2 zone (Figure 1) in between our two-seismic datasets sketching a time slice overview (without specifying the age or

TWT depth) reproducing a similar structure to what is illustrated in Figure 4c,d. They describe the Seagap fault as characterized by a series of restraining and releasing bends, the final geometry of which is related to the reactivation of basement-involved pre-existing fault structure.

In all our scenarios, we are aware we could observe only the shallowest (above 4.5 s TWT) part of the Seagap structure. But a deep ION seismic line (Figure 14, also shown in Figure 3 by Roche & Ringenbach, 2022) allows us to infer that the Seagap fault must root and be controlled by structures below the 4.5 TWT limit of our seismic data. Deeper seismic sections could certainly resolve or unravel the hidden and rooted structure of the Seagap large-scale structure.

5.2 | Kinematic and regional significance of the Seagap fault

Our synthesis of active deformation data from the region places the structural interpretations proposed here within a framework of recent stratigraphic, regional and neotectonic constraints. This new compilation enables us to revisit some hypotheses on the tectonic significance of this large-scale crustal structure. The Seagap structure appears as a long-lived left-lateral strike slip structure that deformed the pre-existing pre-Aptian oceanic

lithosphere and inverted some pre-existing structures (Sauter et al., 2018; Figures 14 and 15). Strain localization in oceanic lithosphere is comparatively rare, as the crust is stronger than continental crust (Burov, 2011). The localized reactivation of ancient crustal-scale transform faults separating lithosphere of different ages may have played an important role; strain localizes at lateral heterogeneities in crustal structure (e.g. Burov & Diament, 1995; Petit & Ebinger, 2000). The former transform faults are loaded by thick sedimentary sequences that may enhance lateral variations in crustal state-of-stress. Important to note is that plate kinematic models of GNSS data suggest that strain is distributed from the Seagap fault to northern Madagascar (Stamps et al., 2020), and this distributed strain may be characteristic of rifting of ancient, comparatively strong oceanic lithosphere. The structural details of such reactivation require more detailed seismicity analyses and crustal imaging below our 4.5 TWT data cutoff.

Overall, the seismic scale structure analysis here suggests that the Seagap fault zone remained a confined and localized discontinuity (Figures 4–8 and 12) that reshaped the upper Mesozoic structure into a system of releasing and restraining bends (Figures 2 and 4). In the late Neogene, the Seagap fault appears to have been reactivated mainly as a normal fault (up to few metres of fault throw, Figure 13), or series of normal fault segments (certainly at the seafloor, Figure 13) but with none of the structural complexity that characterizes the recent evolution of the Davie Ridge (Franke et al., 2015) which evolved from a transform fracture to a ridge transtensional or transpressional structure (see Roche & Ringenbach, 2022 as well as Intawong et al., 2019). Both the Seagap fault zone and the Davie Ridge are zones of active E-W extension, as indicated by abundant M > 4 earthquakes with normal focal mechanisms (e.g. Bertil et al., 2021; Grimison & Chen, 1988; Mulibo & Nyblade, 2016; Nyblade & Robinson, 1994) (Figure 2b).

The second main observation from our interpretation is that the initial kinematic history of the Seagap fault indicates that the structure co-existed with the dextral transform fault activity of the DFZ (until ca. 125 Ma). The DFZ was quiescent until the Late Eocene (Franke et al., 2015; Vormann et al., 2020) when it became very active as an extensional and transtensional ridge structure, creating a series of graben and half-graben structures (Figure 17) including the seismically active Kerimba and Lacerda basins (Figure 2c). The Davie Ridge represents an intensely deformed, broad fault zone. The Seagap fault instead remained active as a localized left-lateral strike slip structure, certainly from at least the Eocene into the upper Neogene, being the only visible large-scale transcurrent fault in the area.
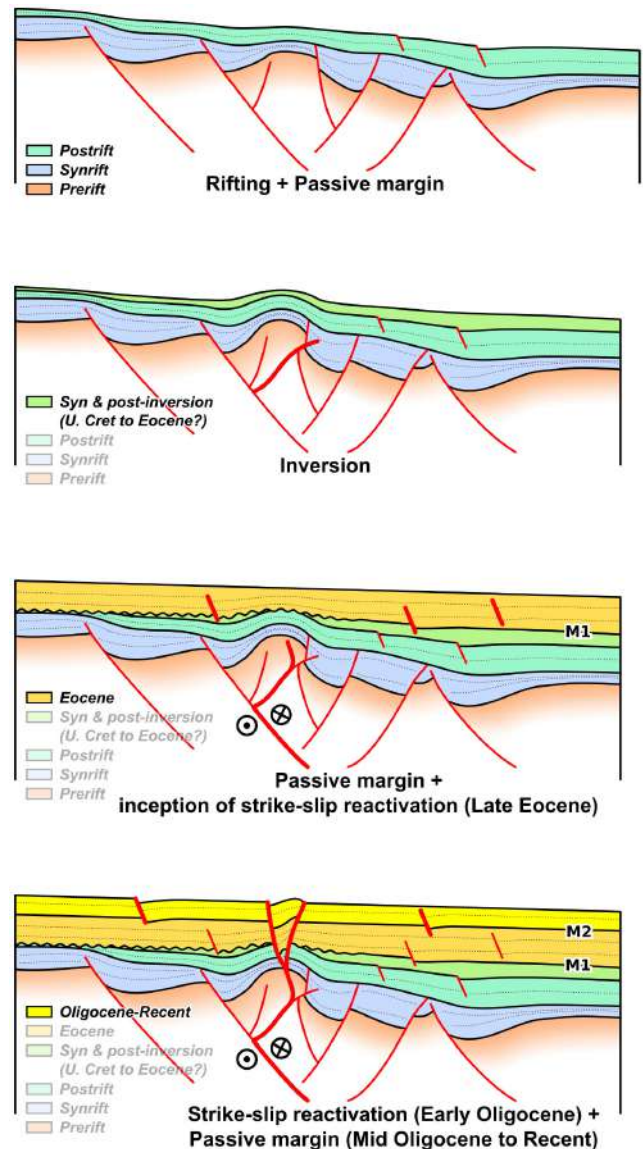
FIGURE 16 Simplified structural model sketching the Seagap fault zone evolution. From top to bottom the (a) lower Cretaceous transtensional structures affecting the Somalian offshore basement (b) upper Cretaceous reactivation by the Seagap fault zone (c) lower to upper Eocene extensional structure (d) Oligocene to Recent Seagap strike slip reactivation.

The Seagap fault never appears displaced or deformed by any of the diffuse rift structures (Figures 4–6, 10, 12 and 17; Dottore Stagna et al., 2022) although in places it appears instead to perturbate the rift distribution. Therefore, the role of the Seagap fault has been with respect both to the initial spreading structure which created the offshore passive margin and the large regional transform structure (Davie Ridge) still an open question. The lack of precise initiation age (Jurassic? Cretaceous?) and the lack of knowledge of its termination (Figure 2) add to the complexity. Some authors (Sinha et al., 2019 but also Roche & Ringenbach, 2022)
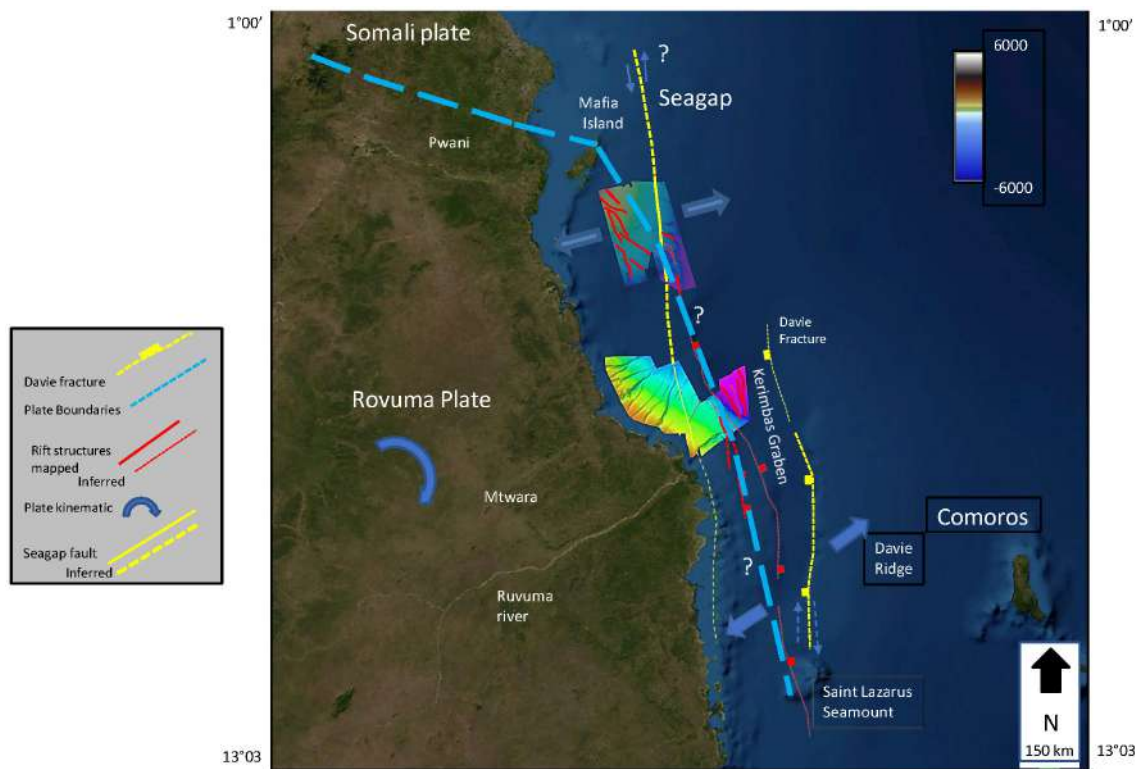
FIGURE 17 Regional offshore Tanzania structure outline. Yellow dot. Seagap fault. Bright yellow dot: Davie fault inferred from literature. Red dotted: Kerimba basin. Red line: Outline of the Neogene extensional fault structure. Thick blue dotted; inferred position of the Rovuma western microplate boundary. Blue arrow: Inferred current extensional (see Delvaux & Barth, 2010)/rotational tectonic in a Nubia-fixed reference frame. (Stamps et al., 2021).

suggested the Seagap fault represents a late (post-Aptian?) offshoot of the Davie Ridge, but the opposite (left-lateral) sense of shear with respect to the DFZ and the lack of ridge type structures poses some issues with their hypothesis (Figure 17). Other authors propose the Seagap fault to be an extension of, and an offshore shift of the EARS as described by Nicholas et al. (2007). In this scenario, as an alternative hypothesis, the recent Seagap history could represent an effect of the counterclockwise rotation of the Rovuma plate (since late Oligocene?) reactivating the broad fracture zones which would fit with a sinistral shear sense of the Seagap fault up to the Neogene (Figure 15). Geodetic strain rate models further confirm the relative clockwise rotation of the Lwandle and Rovuma plates (Saria et al., 2014; Stamps et al., 2018) which then predict a sinistral transcurrent fault.

At present, earthquake slip vectors along the coast of Tanzania and northern Mozambique follow a well-defined belt of seismicity contiguous with the Davie Ridge structures to the south (Bertil et al., 2021; Grimison & Chen, 1988; Mougenot et al., 1986). This relatively narrow zone of seismicity is assumed to delineate a microplate boundary (the Rovuma-Somalia boundary) approximatively traced somewhere

between the coast and the Davie Ridge (e.g. Mulibo and Nyblade, 2016; Saria et al., 2014; Stamps et al., 2018) (Figure 17). Therefore, a hypothesis that could be further explored is that the Seagap fault is part of the Rovuma-Somalia microplate boundary (see reconstruction by Stamps et al., 2020) and the structural expression of their relative rotation. Interestingly, in the offshore Tanzania, Sauter et al. (2018), assign the Seagap fault the role of the Continental-Ocean Transition (COT, Figure 1), although this contrasts with other authors (Roche & Ringenbach, 2022; Sinha et al., 2019) which instead place the COT further east. All these data and related uncertainties underline both the significance of the Seagap fault and its potential role as tectonic expression of the microplate border but also the need for further investigation. Offshore deep seismic sections, seafloor maps, additional dense geodetic data and seismological monitoring data across the Tanzanian coast south down to North Mozambique may help to resolve these uncertainties. The sparse and scattered nature of the offshore subsurface and geodetic datasets that are so far publicly accessible remain the main limiting issues and source of uncertainties behind models proposed in that tectonically active part of the planet.

6 | CONCLUSION

By using 3D seismic data and exploration wells, we investigated the tectonic architecture and evolution of the Seagap fault from the Late Eocene to Present across the Tanzania offshore passive margin. The seismic interpretation, correlations of dated seismic horizons, surface maps and attribute analyses allowed us to reconstruct the regional architecture of the Seagap fault, its polyphase history, and infer its connection to older breakup structures. The following structural and tectonic observations and interpretations have been made:

- The Seagap fault zone represents a long-lived regional structure (Cretaceous to now?) rooted into Mesozoic transcurrent structures.
- It coexisted with the Davie Fracture Zone and was active during most of the Davie Ridge reactivation.
- Presumably from Late Cretaceous through all the Miocene (?), the Seagap fault acted as sinistral strike-slip structure.
- Its structure is expressed by a series of releasing and restraining bends that seismic data reveal as complex reactivated pop up or extensional structures.
- Seafloor data and available focal mechanisms indicate the Seagap fault is currently active mostly as a normal fault system.
- Regional geophysical data but also geodetic data suggest the Seagap fault may represent the Rovuma microplate plate border margin.

PEER REVIEW

The peer review history for this article is available at https://publons.com/publon/10.1111/bre.12716.

DATA AVAILABILITY STATEMENT

The authors confirm that all relevant data are included in the paper. All additional data are available upon reasonable request to the authors.

ORCID

David Iacopini https://orcid.org/0000-0003-4925-9665
Stefano Tavani https://orcid.org/0000-0003-3033-5314
Vittorio Maselli https://orcid.org/0000-0001-7301-0769

REFERENCES

Aydin, A., & Nur, A. (1985). The types and role of stepovers in strike-slip tectonics, The Society of Economic Paleontologists and Mineralogists (SEPM) Strike-Slip Deformation, Basin Formation, and Sedimentation (SP37).

Bassias, Y. (1992). Petrological and geochemical investigation of rocks from the Davie fracture zone (Mozambique Channel) and some tectonic implications. *Journal of African Earth Sciences (and the Middle East)*, *15*(3–4), 321–3311.

Bassias, Y., & Leclaire, L. (1990). The Davie ridge in the Mozambique channel: Crystalline basement and intraplate magmatism. *Neues Jahrbuch fur Geologie und Palaontologie-Abhandlungen*, *2*, 611–110.

Bertil, D., Mercury, N., Doubre, C., Lemoine, A., & Van der Woerd, J. (2021). The unexpected Mayotte 2018–2020 seismic sequence: A reappraisal of the regional seismicity of the Comoros. *Comptes Rendus. Géoscience*, *353*(S1), 1–25.

Burov, E. B. (2011). Rheology and strength of the lithosphere, marine and petroleum. *Geology*, *28*, 1402–1443 ISSN 0264-8172.

Burov, E. B., & Diament, M. (1995). The effective elastic thickness (Te) of continental lithosphere: What does it really mean? *Journal of Geophysical Research*, *100*, 3895–3904.

Chopra, S., & Marfurt, K.(2007). Seismic attributes for fault/fracture characterization. SEG Technical Program Expanded Abstracts. https://doi.org/10.1190/1.2792785

Coffin, M. F., & Rabinowitz, P. D. (1987). Reconstruction of Madagascar and Africa: Evidence from the Davie Fracture Zone and Western Somali Basin. *Journal of Geophysical Research*, *112*, 113105–111406. https://doi.org/10.10211/JB0112iB011p0113105

Coffin, M. F., & Rabinowitz, P. D. (1992). The Mesozoic east African and Madagascan conjugate continental margins; stratigraphy and tectonics. In J. S. Watkins, Z. Feng, & K. J. McMillen (Eds.), *Geology and geophysics of continental margins* (pp. 2011–2240). AAPG Memoir 53.

Courgeon, S., Bachèlery, P., Jouet, G., Jorry, S. J., Bou, E., BouDagher-Fadel, M. K., Révillon, S., Camoin, G., & Poli, E. (2018). The offshore east African rift system: New insights from the Sakalaves seamounts (Davie ridge, SW Indian Ocean). *Terra Nova*, *30*, 380–388. https://doi.org/10.1111/ter.12353

Craig, T. J., Jackson, J. A., Priestley, K., & McKenzie, D. (2011). Earthquake distribution patterns in Africa: Their relationship to variations in lithospheric and geological structure, and their rheological implications. *Geophysical Journal International*, *185*(1), 403–434.

Daly, M. C., Green, P., Watts, A. B., Davies, O., Chibesakunda, F., & Walker, R. (2020). Tectonics and landscape of the central

African plateau and their implications for a propagating southwestern rift in Africa. *Geochemistry, Geophysics, Geosystems*, *21*(6), e2019GC008746.

Davis, J. K., Lawver, L. A., Norton, I. O., & Gahagan, L. M. (2016). New Somali Basin magnetic anomalies and a plate model for the early Indian Ocean. *Gondwana Research*, *34*, 16–210. https://doi.org/10.1016/j.gr.2016.02.010

Delvaux, D., & Barth, A. (2010). African stress pattern from formal inversion of focal mechanism data. *Tectonophysics*, *482*(1–4), 105–128.

Deville, E., Marsset, T., Courgeon, S., Jatiault, R., Ponte, J. P., Thereau, E., Jouet, G., Jorry, S. J., & Droz, L. (2018). Active fault system across the oceanic lithosphere of the Mozambique Channel: Implications for the Nubia–Somalia southern plate boundary. *Earth and Planetary Science Letters*, *502*, 210–220. https://doi.org/10.1016/j.epsl.2018.08.052

Dottore Stagna, M., Maselli, V., Grujic, D., Reynolds, P., Reynolds, D., Iacopini, D., Richards, B., Underhill, J. R., & Kroon, D. (2022). Structural controls on slope evolution and sediment dispersal pathways along the northern Tanzania continental margin, western Indian Ocean. *Marine Geology*, *443*, 106662. https://doi.org/10.1016/j.margeo.2021.106662

Ebinger, C. J., & Sleep, N. (1998). Cenozoic magmatism throughout East Africa resulting from impact of a single plume. *Nature*, *395*, 788–791. https://doi.org/10.1038/27417

Ekstrom, G., Nettles, M., & Dziewonski, A. M. (2012). The global CMT project 2004–2010: Centroid-moment tensors for 13,017 earthquakes. *Physics of the Earth and Planetary Interiors*, *200–201*, 1–9. https://doi.org/10.1016/j.pepi.2012.04.002

Famin, V., Michon, L., & Bourhane, A. (2020). The Comoros archipelago: A right-lateral transform boundary between the Somalia and Lwandle plates. *Tectonophysics*, *789*, 228539. ISSN 0040-1951. https://doi.org/10.1016/j.tecto.2020.228539

Franke, D., Jokat, W., Ladage, S., Stollhofen, H., Klimke, J., Lutz, R., Mahanjane, E. S., Ehrhardt, A., & Schreckenberger, B. (2015). The offshore east African rift system: Structural framework at the toe of a juvenile rift. *Tectonics*, *34*, 2086–2104. https://doi.org/10.1002/2015TC0031122

Gaina, C., Torsvik, T. H., van Hinsbergen, D. J., Medvedev, S., Werner, S. C., & Labails, C. (2013). The African plate: A history of oceanic crust accretion and subduction since the Jurassic. *Tectonophysics*, *604*, 4–25. https://doi.org/10.1016/j.tecto.2013.05.0311

Geiger, M., Clark, D. N., & Mette, W. (2004). Reappraisal of the timing of the breakup of Gondwana based on sedimentological and seismic evidence from the Morondava Basin, Madagascar. *Journal of African Earth Sciences*, *310*(4), 363–3101. https://doi.org/10.1016/j.jafrearsci.2004.02.003

Grimison, N. L., & Chen, W. P. (1988). Earthquakes in Davie ridge-Madagascar region and the southern Nubian-Somalian plate boundary. *Journal of Geophysical Research*, *113*, 10439–10450.

Heirtzler, J. R., & Burroughs, R. H. (1971). Madagascar's paleoposition: New data from the Mozambique Channel. *Science*, *174*, 488–490. https://doi.org/10.1126/science.174.4008.488

Higgins, R., & Sofield, M. (2011). *East Africa transform margin—The view from Tanzania and Madagascar*. 10th PESGB/HGS Conference on African E&P, London.

Intawong, A., Hodgson, N., Rodriguez, K., & Hargreaves, P. (2019). Oil prospects in the Mozambique channel: Where incipient subduction meets passive margin. *First Break*, *37*, 75–81. https://doi.org/10.3997/1365-2397.n0004

Kent, P. E., Hunt, J. A., & Johnstone, D. W. (1971). *The geology and geophysics of coastal Tanzania (Institute of Geological Sciences Geophysical Paper No. 6)*. HMSO.

Klimke, J., & Franke, D. (2016). Gondwana breakup: No evidence for a Davie fracture zone offshore northern Mozambique, Tanzania and Kenya. *Terra Nova*, *210*(4), 233–244. https://doi.org/10.1111/ter.12214

Kusky, T. M., Toraman, E., Raharimahefa, T., & Rasoazanamparany, C. (2010). Active tectonics of the Alaotra–Ankay Graben System, Madagascar: Possible extension of Somalian–African diffusive plate boundary? *Gondwana Research*, *18*(2–3), 274–294.

Macgregor, D. (2015). History of the development of the East African Rift System: A series of interpreted maps through time. *Journal of African Earth Sciences*, *101*, 232–252. ISSN 1464-343X.

Mahanjane, E. S. (2014). The Davie fracture zone and adjacent basins in the offshore Mozambique margin—A new insights for the hydrocarbon potential. *Marine and Petroleum Geology*, *57*, 561–571. https://doi.org/10.1016/j.marpetgeo.2014.06.015

Maselli, V., Iacopini, D., Ebinger, C. J., Tewari, S., de Haas, H., Wade, B. S., Pearson, P. N., Francis, M., van Vliet, A., Richards, B., & Kroon, D. (2020). Large-scale mass wasting in the western Indian Ocean constrains onset of east African rifting. *Nature Communications*, *11*, 3456. https://doi.org/10.1038/s41467-020-17267-5

Maselli, V., Kroon, D., Iacopini, D., Wade, B. S., Pearson, P. N., & de Haas, H. (2019). Impact of the east African rift system on the routing of the deep-water drainage network offshore Tanzania, western Indian Ocean. *Basin Research*, *32*, 789–803. https://doi.org/10.1111/bre.1231110

Mitchum, R. M., Vail, P. R., & Sangree, J. B. (1977). Seismic stratigraphy and global changes of sea level, part 6: Stratigraphic interpretation of seismic reflection patterns in depositional sequences. In C. E. Payton (Ed.), *Seismic stratigraphy—Applications to hydrocarbon exploration* (Vol. *26*, pp. 117–133). Memoir of the American Association of Petroleum Geologist Tulsa. https://doi.org/10.1306/M26490C8

Mougenot, D., Recq, M., Virlogeux, P., & Lepvrier, C. (1986). Seaward extension of the east African rift. *Nature*, *321*(60110), 51111–51603. https://doi.org/10.10310/32151111a0

Mulibo, G., & Nyblade, A. (2016). The seismotectonics of southeastern Tanzania: Implications for the propagation of the eastern branch of the east African rift. *Tectonophysics*, *674*, 20–30. ISSN 0040-1951. https://doi.org/10.1016/j.tecto.2016.02.009

Müller, C. O., & Jokat, W. (2019). The initial Gondwana break-up: A synthesis based on new potential field data of the Africa-Antarctica corridor. *Tectonophysics*, *1150*, 301–3210.

Nicholas, C. J., Pearson, P. N., McMillan, I. K., Ditchfield, P. W., & Singano, J. M. (2007). Structural evolution of southern coastal Tanzania since the Jurassic. *Journal of African Earth Sciences*, *410*, 273–297. https://doi.org/10.1016/j.jafrearsci.20011.04.003

Nyblade, A., & Robinson, S. (1994). The African superswell. *Geophysical Research Letters*, *21*, 765–768. https://doi.org/10.10211/114GL00631

Petit, C., & Ebinger, C. (2000). Flexure and mechanical behavior of cratonic lithosphere: Gravity models of the East African and Baikal rifts. *Journal of Geophysical Research*, *105*, 19151–19162. https://doi.org/10.1029/2000JB900101

Phethean, J. J. J., Kalnins, L. M., van Hunen, J., Biffi, P. G., Davies, R. J., & McCaffrey, K. J. W. (2016). Madagascar's escape from Africa: A high-resolution plate reconstruction for the Western Somali Basin and implications for supercontinent dispersal. *Geochemistry, Geophysics, Geosystems*, *111*, 5036–5055. https://doi.org/10.1002/2016GC006624

Pike, N., Baker, R. G. A., Owen, M. A., Sirju, C., & Garden, I. R. (2015). The Discovery and Appraisal of the Mzia Field, Tanzania, First EAGE Eastern Africa Petroleum Geoscience Forum, 17–19 November 2015, Dar es Salaam, Tanzania.

Rabinowitz, P. D., Coffin, M. F., & Falvey, D. (1983). The separation of Madagascar and Africa. *Science*, *220*(45112), 611. https://doi.org/10.1126/science.220.45112.611

Reeves, C., & de Wit, M. (2000). Making ends meet in Gondwana: Retracing the transforms of the Indian Ocean and reconnecting continental shear zones. *Terra Nova*, *12*(6), 2112–2100. https://doi.org/10.1046/j.1365-3121.2000.003011.x

Reeves, C. V., Teasdale, J. P., & Mahanjane, E. S. (2016). Insight into the eastern margin of Africa from a new tectonic model of the Indian Ocean. In M. Nemčok, S. Rybár, S. Sinha, S. Hermeston, & L. Ledvenyiova (Eds.), *Transform margins: Development, controls and petroleum systems* (Vol. *431*, pp. 21111–21322). Geological Society London, Special Publications. https://doi.org/10.1144/sp431.12

Rego, M. N., Cameron, N., & Boote, D. (2019). Using basin modelling to examine the origin of the hydrocarbons within the deepwater Rovuma Basin of Tanzania, Mozambique and the Comoros. PESGB-HGS Africa E&P Conference, London, 1st-2nd October (Extended Abstract).

Roche, V., & Ringenbach, J. C. (2022). The Davie fracture zone: A recorder of continents drifts and kinematic changes. *Tectonophysics*, *823*, 229188. ISSN 0040-1951. https://doi.org/10.1016/j.tecto.2021.229188

Sadiki, N., Godfray, G., & Msabi, M. (2021). Characterization of the accommodation zones along restraining and releasing bends from analogue modelling simulating the seagap fault, off-shore Tanzania. *Petroleum Research*, *6*(4), 431–442. ISSN 2096-2495.

Sansom, P. (2018). Hybrid turbidite-contourite systems of the Tanzanian margin. *Petroleum Geoscience*, *24*(3), 258–276. https://doi.org/10.1144/petgeo2018-044

Saria, E., Calais, E., Delvaux, D., Hartnady, C. J. H., & Stamps, D. S. (2014). Present-day kinematics of the east African rift. *Journal of Geophysical Research: Solid Earth*, *1111*, 3584–3600. https://doi.org/10.1002/2013JB0101101

Sauter, D., Ringenbach, J. C., Cannat, M., Maurin, T., Manatschal, G., & McDermott, K. G. (2018). Intraplate deformation of oceanic crust in the West Somali Basin: Insights from long-offset reflection seismic data. *Tectonics*, *311*, 51010–51603. https://doi.org/10.1002/20111TC0041100

Sauter, D., Unternehr, P., Manatschal, G., Tugend, J., Cannat, M., le Quellec, P., et al. (2016). Evidence for magma entrapment below oceanic crust from deep seismic reflections in the Western Somali Basin. *Geology*, *44*(6), 4011–4410. https://doi.org/10.1130/g31111411.1

Sayers, N. (2016). Linking recent gas discoveries to their source kitchens, offshore Tanzania. Presented at East Africa: From Research to Reserves, Geological Society, London, 13–15 April 2016, 76–77.

Scrutton, R. A. (1978). Davie fracture zone and the movement of Madagascar. *Earth and Planetary Science Letters*, *311*(1), 104–1010. https://doi.org/10.1016/0012-1021X(1110)110143-11

Ségoufin, J., Munschy, M., Bouysse, P., & Mendel, V. (2004). *Map of the Indian Ocean*. CGMW (Commission for the Geological Map of the World).

Ségoufin, J., & Patriat, P. (1980). Existence d'anomalies mesozoiques dans le basin de Somalie. Implications pour les relations Afrique-Antarctique-Madagascar. *Comptes Rendus de l'Académie des Sciences Série IIa:Sciences de la Terre et des Planètes*, *2111B*, 5–1010.

Sembroni, A., Molin, P., Pazzaglia, F., Faccenna, C., & Abebe, B. (2016). Evolution of continental-scale drainage in response to mantle dynamics and surface processes: An example from the Ethiopian Highlands. *Geomorphology*, *261*, 12–29. ISSN 0169-555X. https://doi.org/10.1016/j.geomorph.2016.02.022

Seton, M., Muller, R. D., Zahirovic, S., Gaina, C., Torsvik, T., Shepard, G., Talsma, A., Gurnis, M., Turner, M., Maus, S., & Chandler, M. (2012). Global continental and ocean basin reconstructions since 200 Ma. *Earth-Science Review*, *113*(2012), 212–270.

Sinha, S. T., Saha, S., Longacre, M., Basu, S., Jha, R., & Mondal, T. (2019). Crustal Architecture and nature of continental breakup along a transform margin: New insights from Tanzania–Mozambique Margin. *Tectonics*, *38*(4), 20110TC005221. https://doi.org/10.10211/20110TC005221

Stamps, D., Calais, E., Saria, E., Hartnady, C., Nocquet, J., Ebinger, C. J., & Fernandez, R. (2014). A kinematic model for the east African rift. *Geophysical Research Letters*, *119*(6), L05304. https://doi.org/10.10211/20011GL03211101

Stamps, D. S., Kreemer, C., Fernandes, R., Rajaonarison, T., & Rambolamanana, G. (2020). Redefining the kinematics of the east African rift system. *Geology*, *29*, 49.

Stamps, D. S., Kreemer, C., Fernandes, R., Rajaonarison, T. A., & Rambolamanana, G. (2021). Redefining East African Rift System kinematics. *Geology*, *49*(2), 150–155.

Stamps, D. S., Kreemer, C., & Saria, E. (2018). A geodetic strain rate model for the east African rift system. *Scientific Reports*, *10*, 1–10. https://doi.org/10.10310/s4151110-0111-11101111-w

Tuck-Martin, A., Adam, J., & Eagles, G. (2019). New plate kinematic model and tectono-stratigraphic history of the east African and west Madagascan margins. *Basin Research*, *30*, 1118–1140. https://doi.org/10.1111/bre.122114

van Wijk, J., Ellis, N., Liu, L., Lowery, C., & Owens, J. D. (2021, December). Reconstructing Paleo-Dynamic Topography of the Ocean Basins: A Somali Basin Case Study. In *AGU Fall Meeting 2021*. AGU.

Vormann, M., Franke, D., & Jokat, W. (2020). The crustal structure of the southern Davie ridge offshore northern Mozambique—A wide-angle seismic and potential field study. *Tectonophysics*, *778*, 228370. ISSN 0040-1951. https://doi.org/10.1016/j.tecto.2020.228370

Vormann, M., & Jokat, W. (2021a). The offshore branch of the East African Rift System: Crustal fabric across the Kerimbas Graben region. *Geophysical Journal International*, *226*(3), 2073–2102. https://doi.org/10.1093/gji/ggab194

Vormann, M., & Jokat, W. (2021b). Crustal variability along the rifted/sheared East African margin: A review. *Geo-Marine Letters*, *41*, 19. https://doi.org/10.1007/s00367-021-00690-y

Weatherall, P., Marks, K. M., Jakobsson, M., Schmitt, T., Tani, S., Arndt, J. E., Rovere, M., Chayes, D., Ferrini, V., & Wigley, R. (2015). A new digital bathymetric model of the world's oceans. *Earth and Space Science*, *2*, 331–345.

SUPPORTING INFORMATION

Additional supporting information can be found online in the Supporting Information section at the end of this article.